Evaluating Methods for Differential Gene Expression And Alternative Splicing Using Internal Synthetic Controls.

Sudeep Mehrotra[1], Revital Bronstein[1], Daniel Navarro-Gomez[1], Ayellet V. Segrè[1], Eric A. Pierce[1,*]

1 Ocular Genomics Institute, Massachusetts Eye and Ear, Harvard Medical School, Boston, MA, 02114, USA

*** Corresponding author:eric_pierce@meei.harvard.edu**

Abstract

High-throughput transcriptome sequencing has become a powerful tool in the study of human diseases. Identification of causal mechanisms may entail analysis of differential gene expression (DGE), differential transcript/isoform expression (DTE) and identification, classification and quantification of alternative splicing (AS) and/or detection of novel AS events. For such a global transcriptome profiling execution of multi-level data analysis methodologies is required. Each level presents its own unique challenges and the questions about their performance remains. In this work we present results from systematic and consistent assessing and comparing a number of widely used methods for detecting DGE, DTE and AS using internal control "spike-in" sequences (Sequins) in RNA-seq data. We demonstrated that inclusion of internal controls in RNA-seq experiments allows accurate determination of lower bounds detection levels, and better assessment of DGE, DTE and AS accuracy and sensitivity. Tools for RNA-seq read alignment and detection of DGE performed reasonably. More efforts are needed to improve specificity and sensitivity of DTE and AS detection. Low expression of isoforms accompanied with sequencing depth does impact sensitivity and specificity of DTE and AS tools.

Introduction

Whole transcriptom analysis using next generation sequencing (NGS) technology is a powerful tool in the study of human disease [1–4]. This technology generally referred to as RNA sequencing (RNA-Seq) allows the detection of various types of changes in expression levels. These mainly include differential gene expression (DGE), differential transcript/isoform expression (DTE) and identification, classification and quantification of alternative splicing (AS) and/or detection of novel AS events [5], [6–10]. To perform such diverse and global transcriptome profiling and sample comparisons requires a multi-level data analysis and applying multiple methodologies and software programs. Starting with quality control of the sequencing reads and read alignment, through data normalization and statistical calculations of significance, each level of analysis presents its unique challenges. For example, confident estimation of expression levels and splicing events can be challenged by presence of sequencing errors impacting accurate read alignment, biases from library preparation methodology and complexities from exons shared by overlapping genes and their isoforms [7] and [11]. Isoform reconstruction and quantification is also a challenging task with short RNA-Seq reads, in particular for large genes with multiple exons [12]. Multiple computational tools/software programs have been generated, each with their own statistical approach and assumptions. Various studies have evaluated the performance of available tools used in RNA-Seq analytical workflows at varying levels. Some are limited to alignment and/or quantification of feature(gene/isoform) expression or characterization of splicing. A few studies performed a comprehensive and systematic analysis of the RNA-Seq data. They highlight strengths and weaknesses of different alignments, DGE, DTE and AS tools (not an exhaustive list); [7, 13–19]. Efforts such as by the Sequencing Quality Control Consortium (SEQC) data set and the synthetic RNA spike-in controls from the External RNA Control Consortium (ERCC) have extended our understanding of the pros and cons of different sequencing protocols, sequencing centers and platforms and data analysis pipeline [20] and [21]. The ERCC RNA spike-in controls contribute mostly to differential gene expression profiling and junction discovery. However, they do not mimic the complexities of the mammalian genomes and are thus less able to support the evaluation of tools aimed at discerning and quantifying splicing events and isoform quantification.

In this study we have used internal control “spike-in sequences” — sequins —to test the current

capabilities and limitations of widely used RNA-Seq analysis tools [22]. The sequins represent full-length spliced mRNA isoforms, modeling both differential gene expression and alternative splicing events [22]. These synthetic RNAs are designed to model complexities associated with human/mouse transcriptome covering a wide range of gene and transcript isoform expression levels. We added sequins to five (5) different tissues; retinal pigment epithelium (RPE), retina, brain, muscle and kidney from a model organism, mouse, with consistent and realistic sample replicates. We evaluated the performance of the following tools for RNA-seq read alignment - STAR [23] and HISAT2 [24], gene expression quantification - featureCount [25] and HTSeqCount [26], differential gene expression - DESeq2 [27] and edgeR [28], isoform quantification: RSEM [29] and Kallisto [30], differential transcript/isoform expressions - EBSeq [31] and Sleuth [17], and alternative splicing detection - JunctionSeq [32] and MAJIQ [33].

We demonstrate that inclusion of internal controls in RNA-seq experiments allows accurate determination of detection levels, and better assessment of DGE, DTE and AS accuracy. These analyses show that gene expression profiling and DGE tools were found to be robust. The isoform expression profiling tools were robust, but not as tolerant to lower depth of coverage (DOC) as the DGE tools. We recommend high, for confident prediction of differential isoform expression. Even with high DOC, for AS event detection, we found the current tools lacking high sensitivity. This was compounded by lower depth of coverage. More efforts are needed to improve specificity and sensitivity of DTE and AS detection.

Materials and Methods

Data Sets: Isolation & Sequencing

The RNA-Seq data used for the analyses described were generated from tissue of mice with targeted disruption of the *Prpf31* gene [34] and [35]. Total RNA was extracted from retinal pigment epithelium (RPE), retina, brain, muscle and kidneys of 5 *Prpf31*$^{+/-}$ and 4 wild-type littermate male mice (C57BL/6J genetic background). Immediately following euthanization with Co_2, brain muscle and kidney were dissected, washed in PBS and flash frozen in liquid nitrogen. Tissues were lysed using Geno/Grinder (SPEXSamplePrep Metuchen, NJ, USA). Eyes were enucleated and RPE and retinas were isolated as previously described by Fernandez-Godino et al. [36]. Isolated retinas and RPE monolayers

were collected into buffer RLT and placed into -80C. Total RNA was extracted from brain, muscle and kidney using RNeasy maxi kit and from retinas and RPE using RNeasy mini and micro kits respectively (Qiagen, Hilden, Germany) following the manufacturer instructions. RNA was quantified using Qubit (ThermoFisher scientific Waltham, MA, USA) and quality was assessed using a Bioanalyzer (Agilent Santa Clara, CA, USA). RIN numbers were >7 for all the samples.

Data Sets: Library Preparation & Sequencing

For each retina, brain, muscle and kidney sample, 1μg of total RNA was spiked with 1.2ng sequins (v2) controls. For RPE samples 100ng total RNA was spiked with 0.12ng sequin controls. Sequins "MixA" was added to all the wild type (WT) samples and "MixB" to mutant type (MUT) samples. A stranded, paired-end (PE) TruSeq stranded total RNA (Illumina San Diego, C, USA) library preparation was performed. Ribosomal RNA was removed with the Ribo-Zero Human/Mouse/Rat kit. Samples were multiplexed across five different flow cells and were consecutively sequenced. The sequencing was carried out on Illumina HiSeq 2500 Sequencer for 101 cycles at the Ocular Genomic Institute (OGI), Boston, MA (USA).

Preprocessing and Sample Quality Control

Each section of the analysis pipeline was run on a local High Performance Cluster (HPC) with SunGird Engine, 12 compute nodes each with 16 core processor (2X8) and 128 GB memory and the Ocular Genomic Institute (OGI), Boston, MA (USA). First we performed preprocessing of the data set. The quality control/quality assurance (QC/QA) of the data set at lane and samples level. Our aim was to identify any lane level or sample biases in pre-processing of the sequenced reads.

The quality of the sequenced reads was evaluated using FastQC and further collated and summarized using MultiQC [37], [38]. Post merging, an in-house Perl script was used to check and filter out reads with presence of adapter and ambiguous character, 'N'. The Bowtie2 aligner was used to identify ribosomal contamination [39]. Reads aligned to rRNA reference sequences were dropped from all downstream analysis using SAMtools [40]. The mouse (*Mus musculus*) reference sequence was downloaded from Ensembl and annotation files from GENCODE. Supplementary Table S1 lists all the reference databases along with the versions that were used in the analysis. Additionally, Supplementary Table S2 shows all the analysis tools along with versions that were used. Post alignment,

featureCount was used to generate gene expression matrix [25] . To identify possible mixing/mismatch, the normalized read counts were used for clustering of all the samples using Spearman correlation. In summary no lane level or sample level biases were observed. No samples mixing was detected (data not shown).

Comparative Analysis

In the paper performance of various tools used in RNA-Seq work flow are analyzed. All possible combinations of aligners, gene expression profiles, differential genes and isoform expression tools are analyzed. Following sections expands on the tools used in the analysis.

Overview of Sequins

A suite of synthetic RNA isoforms, termed "sequins" (sequencing spike-ins) representing full-length spliced mRNA isoforms, which are entirely artificial sequence and bore no homology to natural reference genomes (human/mouse) have been designed by Hardwick et al. [22]. They align to gene loci encoded on an artificial *in silico* (IS) chromosome. The sequins can be concatenated with the genome of interest (such as human and mouse) and coindexed for alignment. In total, there are 78 artificial gene loci encoding 164 alternative isoforms comprising 869 unique exons and 754 unique introns. Genes ranged from single-exon to large multi-exon loci, with individual isoforms ranging in size from ∼280 bp up to ∼7 kb and comprising up to 36 exons. For more information please refer to [22].

Overview of Analysis Tools: Aligners

The aligners are central and primary in any RNA-Seq analysis. Two different state-of-the-art splice site aware aligners, STAR and HISAT2 were used for alignment [23] and [24]. The alignment was performed using default settings. The STAR aligner was used to align in two-pass mode within the sample and across replicates for each sample set. Respective indexes were created for the mouse reference as per the manual. During preprocessing and QC/QA the reads were aligned using STAR.

Overview of Analysis Tools: Gene Expression

Identification of differentially expressed genes between case and control is vital to many RNA-Seq studies. The first step in this process is creation of a count based profile of expressed genes. A profile refers to genes its read counts across all the samples and conditions. In this study featureCount (from the subRead package, and sometimes referred to as "subRead" in the paper) and HTSeqCount (htseq-count) were used to build gene expression matrices [26]. Mostly, default settings were used for HTSeqCount, calibrating on parameters for reverse-stranded and PE reads as required. The following non default settings for featureCount were applied: (i) reads must be paired (ii) both the pairs must be mapped (iii) use only uniquely mapped reads (iv) multi-mapped reads are not counted and finally (v) chimeric reads are not counted.

We show Pearson's correlation of determination (R^2) via Anaquin or using R. In come cases, marked appropriately, for correlation and other plots the transcripts per million (TPM) for each sample or mean TPM values across the appropriate genotypic replicates were used. All the correlation plots were made using "Corrplot" [41].

Overview of Analysis Tools: Differential Gene Expression

DESeq2 and edgeR are R/Bioconductor packages and were used for differential gene expression (DGE) analysis [27]. Both the tools were used with default parameters. Both the tools apply a negative binomial generalized log-linear model to identify differential expression between experimental conditions.

Overview of Analysis Tools: Isoform Expression

As with genes, identification of expressed transcripts requires creation of expression profiles. For isoform analysis, RSEM and Kallisto were used [29] and [30] . For RSEM we used alignments from Bowtie2 (default for RSEM), STAR and HISAT2 aligners as input to create isoform expression profiles. Kallisto intrinsically uses a "pseudo-alignment" approach distinct from splice site aware aligner (STAR/HISAT2) for detection of isoform expression. In all the tools, calibrations to the parameters were made for reverse-stranded and PE reads. As with genes, for correlation and other plots the read counts were first converted to TPM and mean values were used.

Overview of Analysis Tools: Differential Transcript/Isoform Expression

For differential transcript/isoform expressions, EBSeq and Sleuth were used. RSEMs expression profile matrix were used as input for EBSeq while Kallsito's output were input to Sleuth for DTE. EBSeq applies the Bayesian empirical approach for DTE. Sleuth relies on variance decomposition to better capture the biological differences in transcript, applying shrinkage to stabilize variance across samples replicates [17] for quantification. Both EBSeq and Sleuth were used with default parameters. Note that Sleuth use likely-ratio-test (LRT) in default mode which does not produce LFC values. It allows "Wald" testing as well. We followed the same methodology as described by Pimentel et al [17] for data preparation for LFC and receiver operating characteristic (ROC) for comparison.

Overview of Analysis Tools: Alternative Splicing

We used count-based methods that include both exon-based and event-based approaches. In exon-based methods, read counts are assigned to different features, such as exons or junctions. JunctionSeq is an R/Bioconductor package that applies such an approach and is capable of detecting novel exon junctions. "Differential usage" (DU) is an observed phenomenon in which individual exons or splice junctions display expression that is different with the overall expression of the gene [32]. Hence, the limitation of JunctionSeq is it that it does not make any inference on the type of the splicing event in classical terms such as; Exon Skipping(ES), Intron Retention (IR), Mutually Exclusive Exons (MXE), Alternative $5'$ Splice Sites (A5SS), Alternative $3'$ Splice Sites(A3SS), Alternate first exon (AF) and Alternate last (AL) exon, which are easier to interpret in the biological and universal manner. In an event-based method, splicing events are quantified by calculating the percentage spliced in (PSI) values for each event by measuring the differences in the fraction of junction reads, followed by calculation of difference in PSI (dPSI) between experimental conditions. MAJIQ (Modeling Alternative Junction Inclusion Quantification) [33] uses a local splicing variations (LSVs) approach to detect and quantify RNA splicing. The event detection terms utilized by MAJIQ are restricted to ES, IR, A5SS and A5SS. MAJIQ uses a Bayesian approach and reports posterior probability per LSV as confidence values. Another tool, rMATS [42], is also an event-based method for splice detection and uses a likelihood ratio test to calculate the *P* value and examines whether the between-group differences of mean PSI exceed a given, user-defined threshold. Non-default settings for minimum

of 5 reads for junction detection and 10 reads for the calculation of dPSI. Additionally, calibrations to the parameters were made for reverse-stranded and PE reads. Using sequins sensitivity and specificity of every parameter can be tested. However such an analysis is beyond the scope of this paper. We focused on the systematic reporting of the event across and the tissues and the location rather than on the type of AS events.

Downsampling

To explore impacts of lower depth coverage (DOC) on DGE, isoform expression and AS events, we titrated the original unique alignments into random 150, 100 and 50 million set. The downsampling was performed on RPE, retina and brain samples. For each sample regardless of the genotype we first determined the samples that can undergo downsampling. Not all samples had enough depth of coverage to meet the criterion to downsample. In such instances, the entire sample was used. To ensure proper sequins ratio, for each of these samples, observed (post downsampled) total sequins counts was extracted and compared with the original set. We changed the "seed" during random selection for downsampling.

Results

The RNA-seq data used for the analyses described below were generated from total RNA extracted from RPE, retina, brain, muscle and kidney of mice with targeted disruption of the *Prpf31* gene and littermate controls. Mutations in the *Prpf31* gene cause inherited retinal degeneration [35]. In *Prpf31*$^{+/-}$ mice this manifests as cell autonomous defects in retinal pigment epithelial (RPE) function [43]. Two different concentration mixes of sequin spike-in controls were included in the RNA samples isolated from 5 tissues of the mutant and control mice with 5 and 4 replicates respectively (Methods).

We used these RNA-seq data to comprehensively evaluate landscape of various bioinformatics tools used in RNA-Seq experiment from read alignment to gene expression quantification and their differential analysis, isoform expression quantification and their differential analysis and alternative splicing detection. The strategies and various analysis tools used for comparative analysis in this paper are illustrated in Figure 1.

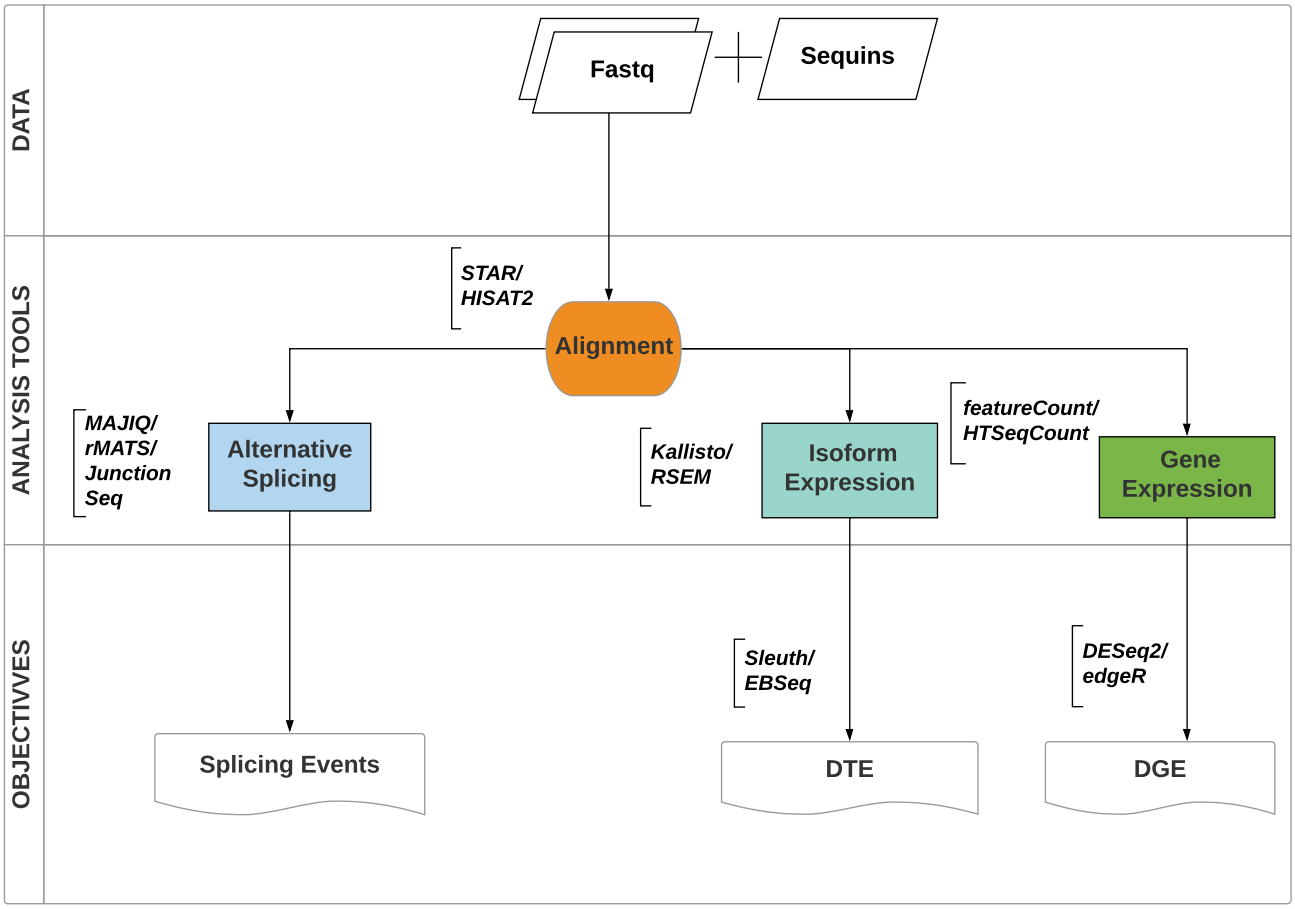

Figure (1) Experimental design flow chart. Top: The RNA-Seq data in the form of fastq files were used as input to alignment tools. Post alignment, different combination of software programs were used for gene expression, isoform expression profiles were created including detection of splicing events, with objective to perform different gene expression (DGE), differential transcript expression (DTE) and differential splicing events.

Sequencing Quality

Since the samples were multiplexed and were consecutively sequenced across 5 flow cells, we tested for any lane biases so as to avoid additive biases that can occur following merging of the reads. During QC/QA aspects such as: total raw reads, sequence quality, total number of bases, GC content, the presence of adaptors and overrepresented k-mers in order to detect sequencing errors, PCR artifacts or contaminations are paid particular attention. Supplementary Figure S1 shows total raw reads including a comparative with high quality (HQ) read set post QC. Here, reads and bases that underwent robust QC process are referred to as HQ. Post QC, 98%–99% reads were retained across all the sample set for all the tissues. Furthermore, Supplementary Table S3, Table S4,Table S5,Table S6 and Table S7 shows the mean, first and third quartile values of each sequencing run. Overall no lane level biases were observed. Supplementary Figure S2 shows mean

per cycle per base quality. The data used for subsequent analyses contained high base quality data.

Sequins In Samples

Sequins are provided as two mixes which differ in gene expression, transcript isoform usage and levels [22]). In this study, mixA was added to all the wild-types sample replicates and mixB to all the mutant sample replicates for all the mouse tissue types. Table 1 shows the final average ratios of sequins across the mouse tissues and genotypes.

Table (1) Detected average sequins ratio in case and control samples. The detected ratios are shown for each mouse tissue. With exception of brain tissue where a disproportionate of the two sequins mixtures were observed. About 35% of the mixA reads for mutants and 65% of mixB reads for the wild types were observed. In all the other tissues, equivalence of the two mixes was observed. IS refers to artificial sequins *in-silico* (IS) chromosome.

Tissue/Ratio	**RPE**	**Retina**	**Brain**	**Kidney**	**Muscle**
%Avg Ratio MUT:WT	3.4**:**3.9	4.2**:**4.5	2.7**:**5.0	3.9**:**4.5	3.8**:**4.2

Two sequin genes from the original set were identified to be inconsistent (confirmed by personal communication) and were removed from the set (gene model file). Supplementary Table S8 shows sequins for gene expression and DGE. All the 76 true positive (TP) genes, for upregulation, downregulation and uniform (no change) are shown. The table shows expression values in original attomoles/μl units. Similarly, Supplementary Table S9 shows the TP set of sequins for DTE. Concentration shown are the same as genes. Finally, Supplementary Table S10 shows TP sequins for AS events. In total we have 28 TP events. However, regardless of the use of aligner, 6 sequins (colored in the table), were not well covered, we did not penalized sequin genes for the lack of coverage. We revised the TP counts for AS events to 22. Supplementary Figure S3 and Figure S4 shows the coverage plot for one such sequin gene, R1_62. This is not among the lowest concentrations (8th highest concentration). For brevity of the 6, one(1) such gene with low coverage is shown. The remaining low coverage genes are reflective of this (R1_62) sequin gene.

Consistencies of the Aligners

Two aligners, STAR and HISAT2 were used for the alignment for all the five tissue types. Figure 2 shows the unique alignment rate from the two aligners using two representative samples; RPE and

retina. The alignments were performed to the mouse genome and to the sequins artificial chromosome (IS).

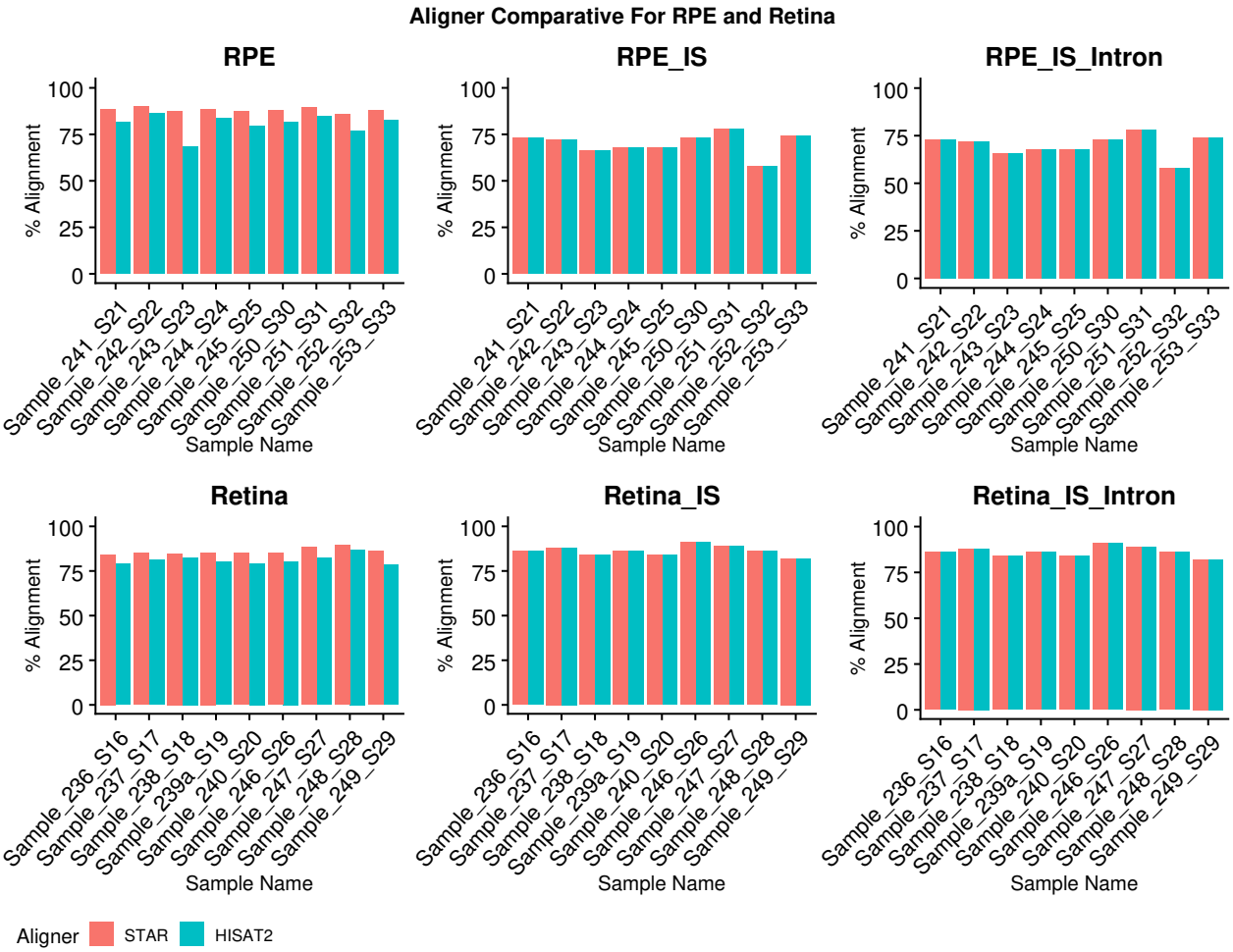

Figure (2) Comparative alignment rate for all the replicates. The figure shows genomic unique alignment, alignment to the sequins artificial chromosome (IS) and intron sensitivity (IS), as reported by STAR and HISAT2 for all the RPE and retina mouse tissues. Overall the alignment rates were indistinguishable. Assigned unique sample identifier assigned to each sample is shown in the x-axis and percentage alignment rate on y-axis. From left to right, first 5 are mutants followed by 4 wild type samples. Supplementary Figure S5 shows genomic alignment, Figure S6 shows alignment rate to *IS* and Figure S7 shows intron sensitivity from the two aligners for all the five mouse tissues.

Since the intron boundaries for the sequins are known, using Anaquin, intron sensitivity was also calculated. Here, sensitivity indicates the fraction of annotated regions covered by alignments of the reads as reported by the aligners. Supplementary Figure S5 shows genomic alignment, Figure S6 shows alignment rate to *IS* and Figure S7 shows intron sensitivity from the two aligners for all the five mouse tissues. Proportionate alignment percentage was observed from both the aligners for all the tissues irrespective of the genotypes and the references.

In the gene model for the spike-in sequences, total sequin gene counts and their relative expression

values are known. We used this information to determine following quantitative and qualitative values: limit of detection (LOD) and limit of quantification (LOQ), correlation of determination of the expected versus observed expression values and finally, correlation of determination of log-fold-changes (LFC) and their proportions across the five different tissue types. Over the next few sections aforementioned aspects are explored and results are presented.

Concentration Levels and High Gene Expression Correlation

The two performance characteristics related to analyte stability, LOD and LOQ were analyzed for all the five tissues sample replicate sets using Anaquin (see [22] and [44] for more details). Figure 3 shows correlation and slope for mouse RPE. This tissue had the lowest depth of coverage amongst all the tissue types and hence was selected as a representative sample set for LOD and LOQ reports. No LOD and LOQ were reported for all the remaining mouse tissues.

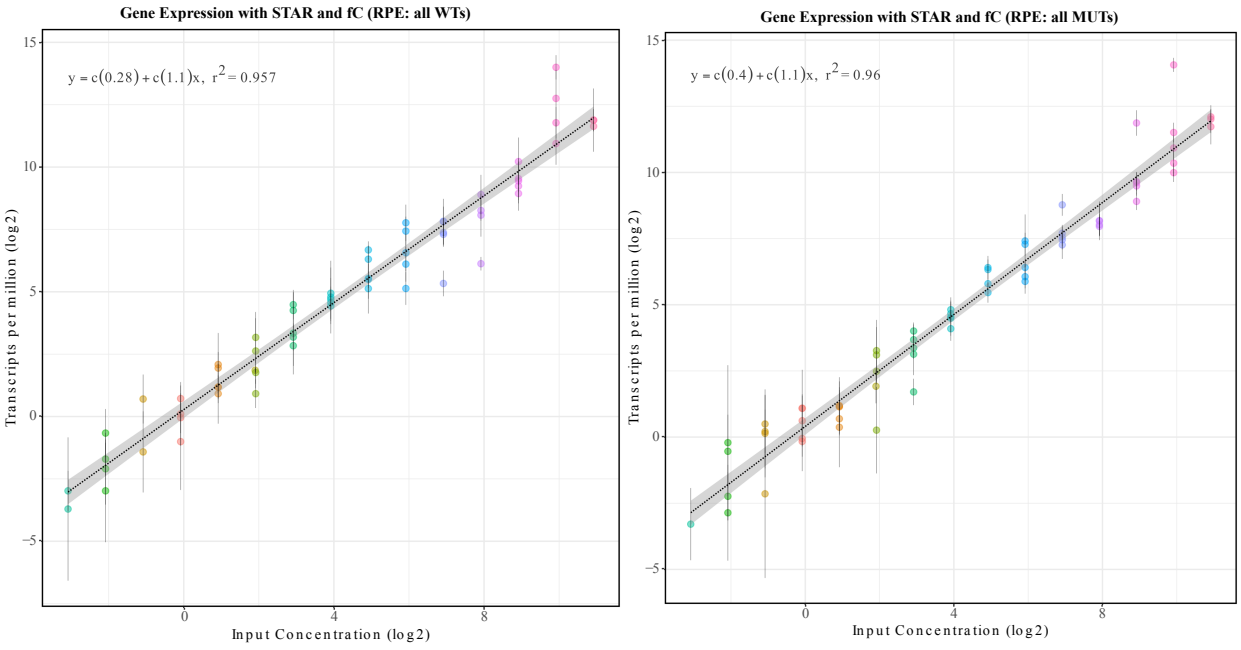

(a) All replicates of wildtype samples, R^2=0.95 (b) All replicates of mutant samples, R^2=0.96

Figure (3) Correlation plot for comparative analysis across all the mouse wild type tissues (a) and mutant tissues (b). Slope, correlation, LOD and LOQ determination using STAR is shown. Known concentrations are on the x-axis and observed concentrations in TPMs is shown on the y-axis. Both the axis are log2 scaled. The vertical bar shows for each sequin genes shows the spread of the concentration values. No LOD or LOQ was detected for this sample set. Few sequin genes were either under or over represented from the slope. fC refers to featureCount.

Next, we calculated R^2 to determine how well, post alignment, read counting tools; featureCount and htseq-count are able to capture the features and their expression values across the sample replicates.

Indeed, all combinations of aligners and read counting tools provided the same high correlation across all samples. Figure 4 and Supplementary Figure S8 show correlation values across the WT and MUT replicates respectively using all possible combinations of the aligners and read counting tools.

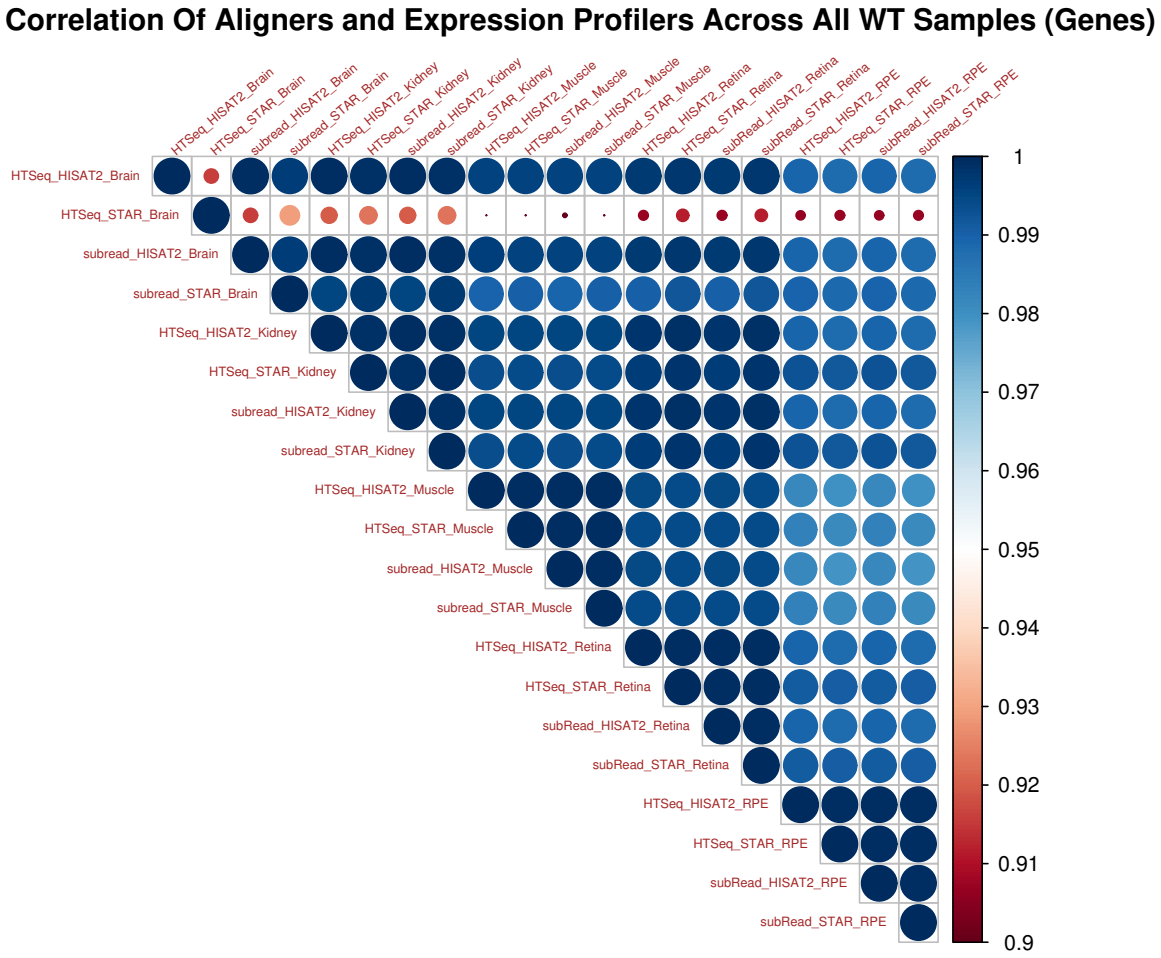

Figure (4) Correlation plot for comparative analysis across all the wild type tissues. An upper triangular heatmap shows high correlation across different combinations of the aligners and genes read counting tools across the five mouse tissues and the replicates. The average TPM values across the replicates were used to calculate the Pearson correlation. The combinations of tools used are shown in the format of: Gene Expression Profile_Aligner_Tissue. The brain samples were impacted by disproportionate sequins ratios.

High Differential Gene Expression Correlation and Proportion

Our next objective was to analyze differential gene expression across all the tissue types and case and controls set. For these analyses, we computed the correlation values for two different DGE tools, edgeR and DESeq2. Sequin genes are added in a known concentration across the tissues,

hence we can examine the correlation of gene expression (LFC) across different tissues. Figure 5 shows an upper triangular computed correlation of determination in the form of a heatmap.

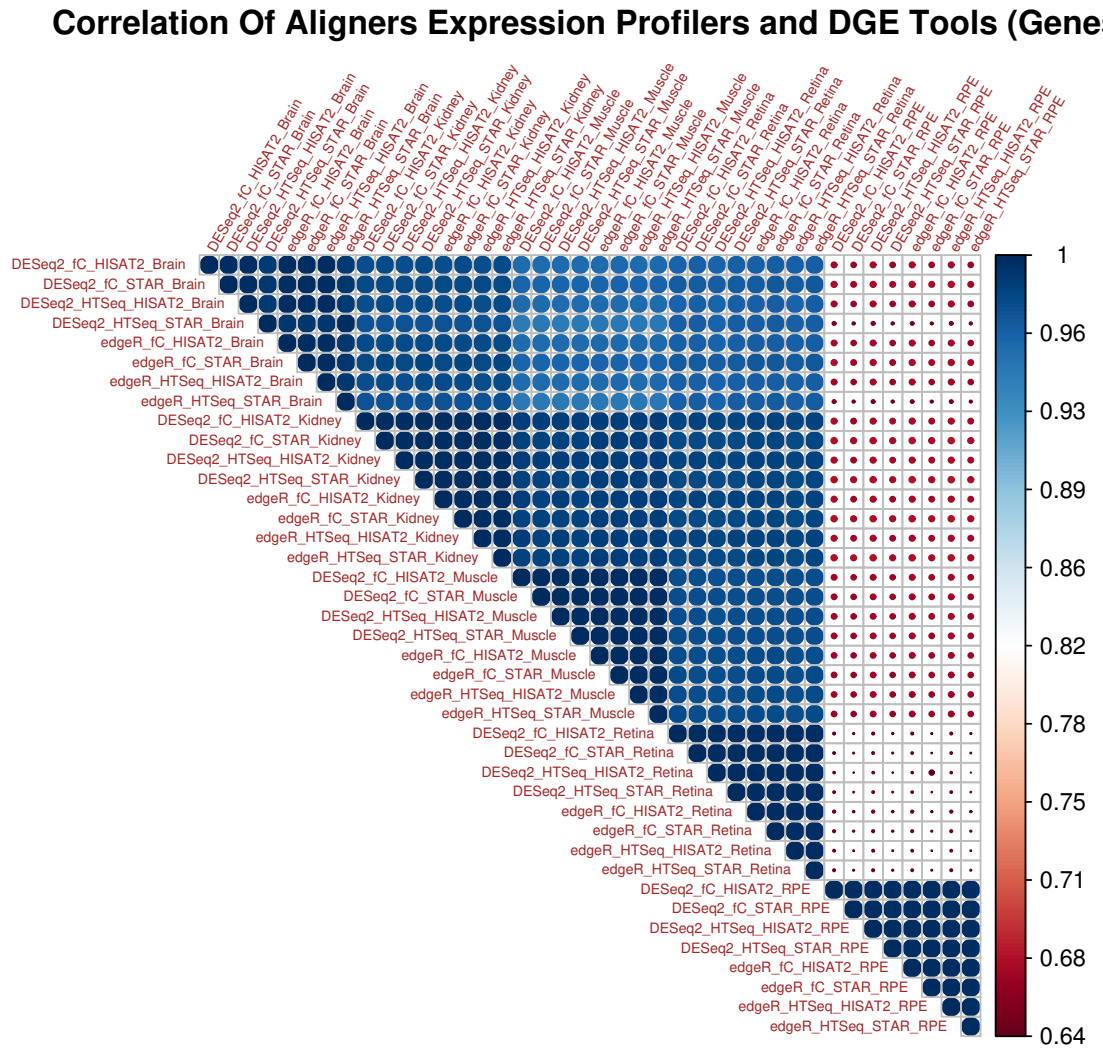

Figure (5) Correlation plot for comparative analysis using two aligners, two read counting tools and two DGE tools across all the mouse tissues. An upper triangular heatmap is generated showing Pearson correlation of determination values using average TPM expression values across the five mouse tissues in the order; brain, kidney, muscle, retina and RPE. The combinations of tools used are shown in the format of: DGE_Gene Expression Profile_Aligner_Tissue, for example, DESeq2_fC_HISAT2_Brain. High correlation of determination values were observed across different tissues types and combinations of different tools with two exception. Correlation of RPE and brain showed the lowest correlation of determination values with other samples. Lower coverage impacted the RPE samples and unequal sequin ratio impacted the brain sample set.

The figure shows (R^2) values for all possible combinations for the two aligners, two feature read count tools, and two differential gene expression analysis tools across all the five mouse tissues. Overall high correlation of determination values were observed regardless of tissues and tools used. The RPE and the brain samples showed lower values compared to other tissues. For RPE this is

likely due to reduced depth of coverage and the brain samples were impacted by disproportionate sequins ratios.

Next, we investigated proportion and directionality of LFC values across all the mouse tissues. Intuition would suggest that for an artificial set of genes, the LFC values and directionality should be proportionate and unidirectional regardless of the mouse tissue type if the depth of coverage is comparable and the ratios of the artificial gene sets were added equally. Figure 6 shows proportions and directionality of sequin genes across all the mouse five tissues. The values shown are sorted based on actual LFC values. Some inconsistencies in the directionality and LFC proportions were observed.

In the brain samples, there were set of sequin genes that showed disproportions and changes in directionality. This was mostly observed for sequin genes with ground truth of LFC 0 (zero). Such genes were over or under represented (upto 2 units in either direction). Three sequins were not reported. In the kidney dataset, we observed loss of 2 sequins.

The underlying expected fold changes between the case and control sample sets is known, we can gauge the sensitivity and specificity of various combinations of the tools using receiver operating characteristics (ROC). Figure 7 shows the ROC curve for all the mouse tissues with different combinations of all the analysis tools.

Each plot in the figure for a given tissue shows the performance of different combinations of the tools used for the alignments, gene expression values and DGE. All show high accuracy with the different combinations aligners, feature read counting and DGE tools tested. The brain sample set was an exception compared to the rest of the samples. The shift in the curves for certain combinations of the tools was due to missed reporting of the sequin genes. The same was observed with the kidney samples. All the other combinations of the tools showed a great balance between sensitivity and specificity. We further investigated the brain and kidney samples to better identify combinations of the tools with drop in performance was observed (Figure S9). Disproportionate ratio of the two sequins mixtures impacted the sensitivity for the brain sample. Loss of 2 sequins in the kidney sample caused the shift ROC.

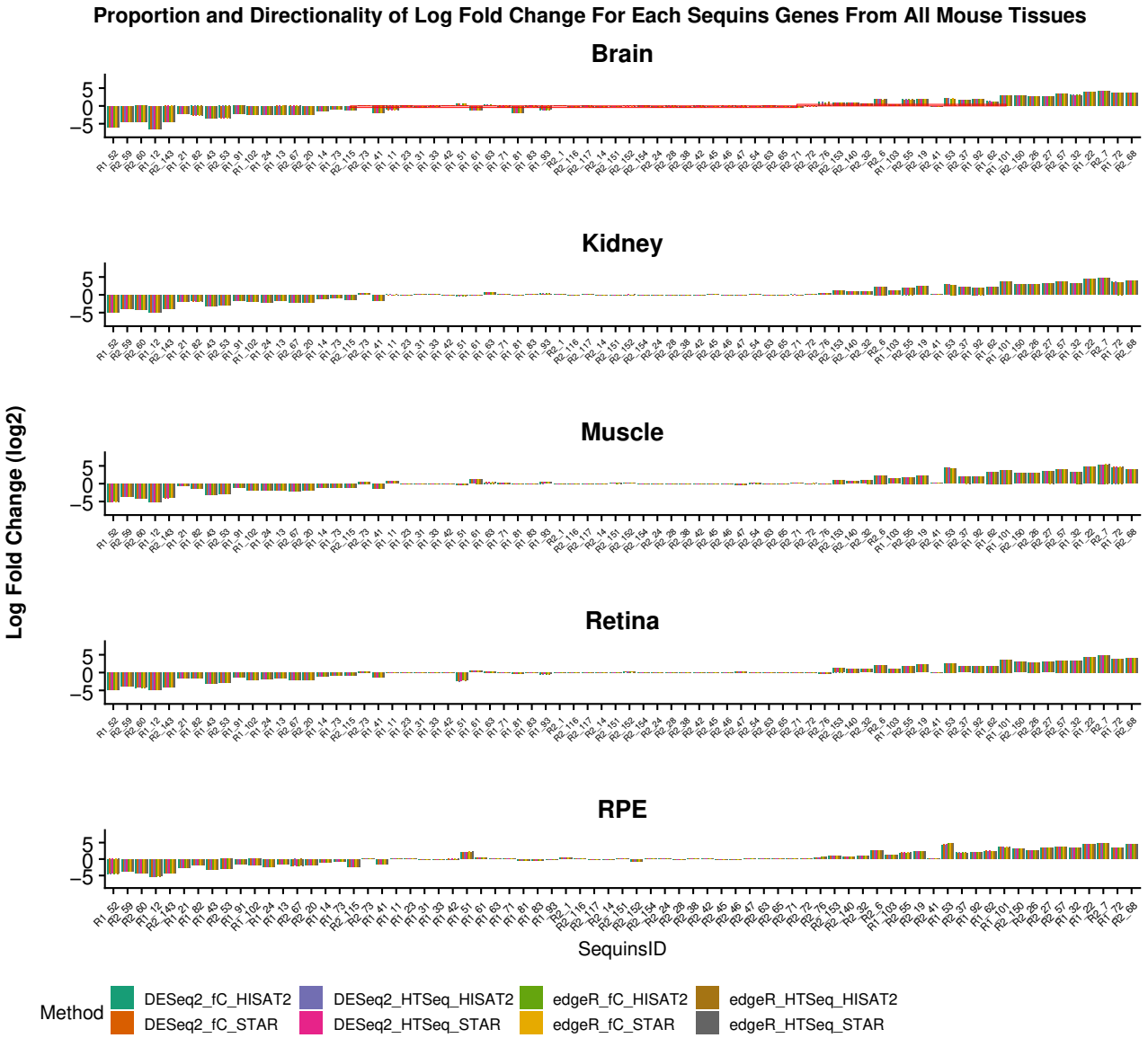

Figure (6) Comparative proportion of log-fold-changes for the sequin genes across all the mouse tissues using different aligners, read counting and DGE tools. In the x-axis all the sequin genes are shown and LFC values (log2) is shown on the y-axis. The values shown are sorted based on actual LFC values. In the top panel, the brain sample highlights three sections (red rectangle boxes) that show some difference in the proportions and in some cases directionality across all the tissues. In most cases, discrepancies in the proportionality and directionality was impacted for sequin genes that should have no (zero) LFC values. In such cases, some marginally over or under LFC values are reported (at most by 1 unit). For example R1_51 was reported 2 units higher in RPE and the same was 2 unit lower in retina. Actual LFC is 0. R1_21 should show about -3 LFC, however in muscle it is barely reaching ∼ -1. Sequin R1_51 was not reported by some combinations of the tools in the kidney and brain samples. The brain sample set shows the most inconsistent results compared to the rest of the mouse tissues. fC refers to featureCount from the subRead package, HTSeq refers to HTSeq-Count.

High Isoform Expression Correlation

For isoform expression analysis we used different combinations of alignment tools along with an orthogonal approach. We used RSEM with BowTie2 and RSEM with the STAR aligner as a standard

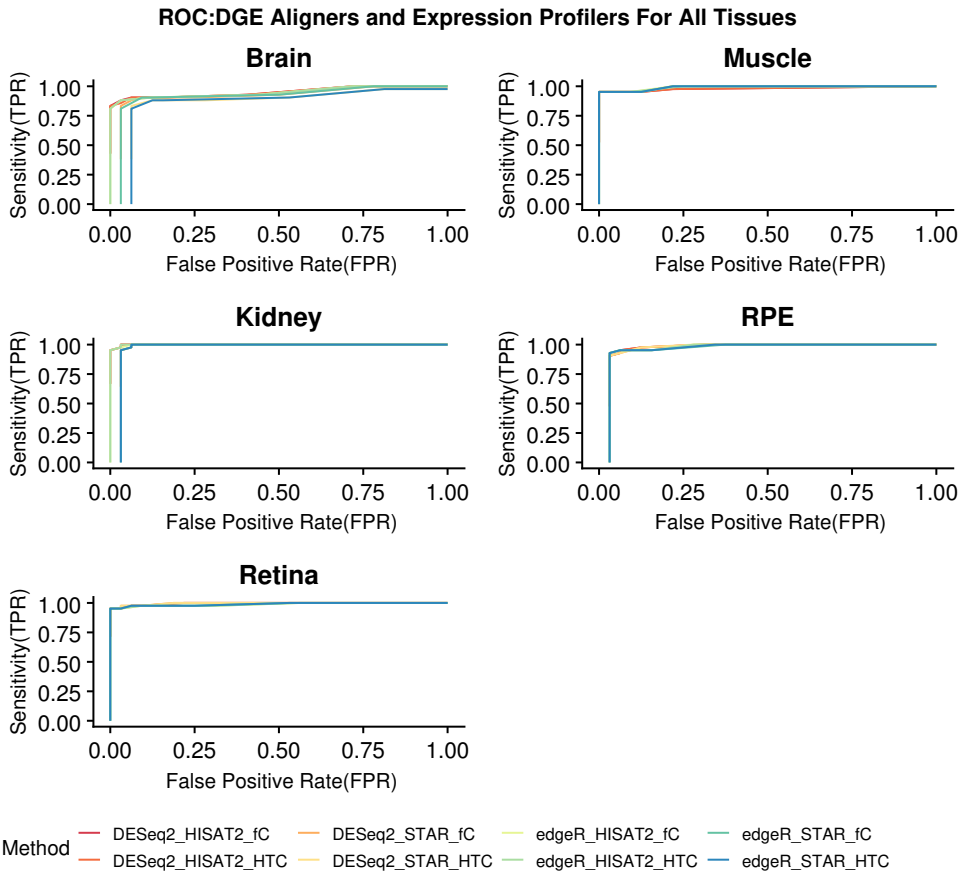

Figure (7) ROC (receiver operating characteristic) curves for Sequin genes for diagnostic performance in measuring fold change. Each plot reflects the performance of different combinations of the aligners, feature read counting and DGE tools. The brain sample set shows an exception compared to the rest of the tissues. The visibility of all the combinations is impaired by the fact that in many cases the results were identical and hence overlapping. fC refers to featureCount from the subRead package, HTC refers to HTSeq-Count.

approach for detecting isoform expression, and Kallisto's unique pseudo-alignment approach as an orthogonal approach. We performed multilevel analysis to gauge performance of analyte stability, LOD and LOQ along with correlation of expected vs observed for the isoforms. Figure 8 shows the correlation plot for the mouse RPE WT samples using RSEM and Kallisto. No LOD and LOQ was reported for any of the mouse tissues via any combination of the tool. Some isoforms showed greater expression variability, but remained non specific to any particular tissue types. Figure 9 shows an upper triangular computed correlation of determination in the form of a heatmap for all the wildtype dataset. Simialr observations were made for the mutant sample set (Supplementary Figure S10). The figure shows (R^2) values for all possible combinations for the two aligners (STAR and BowTie2), "feature" read count tool (RSEM), and Kallisto across all the five mouse tissues. Overall high correlation of determination values were observed regardless of tissues and tools used.

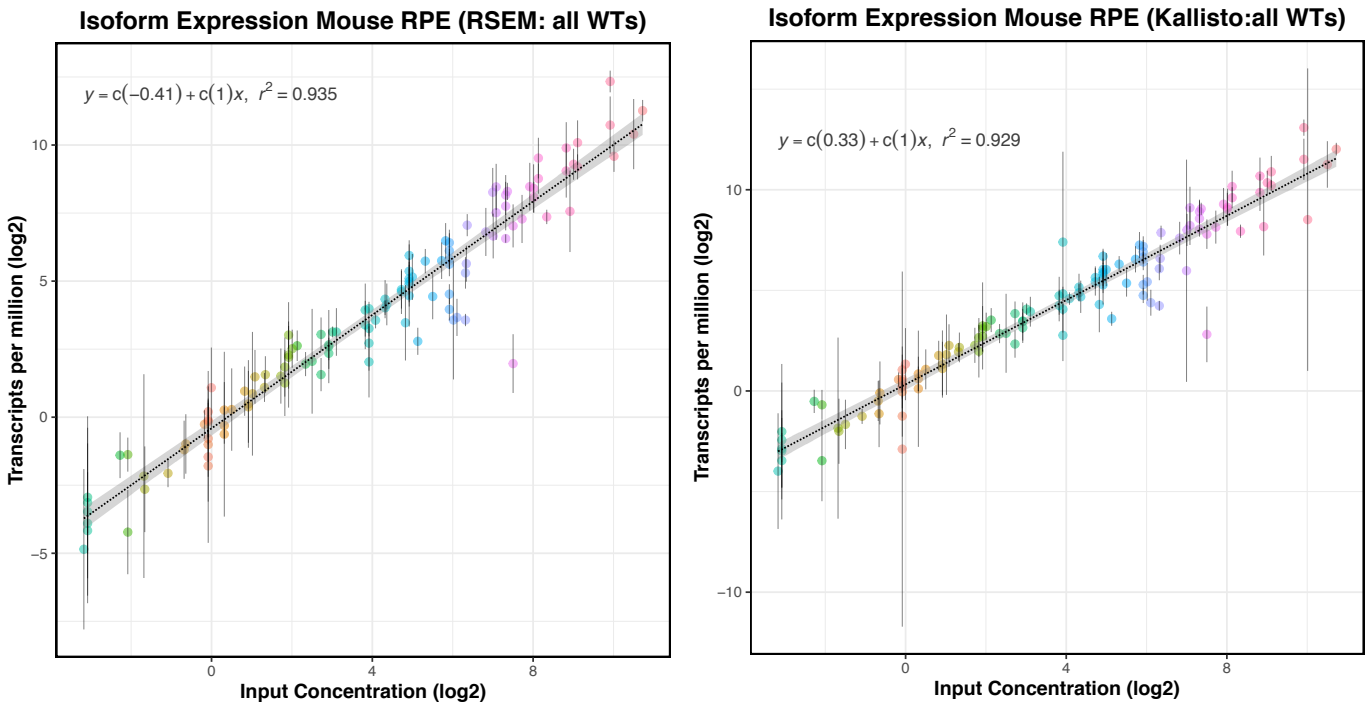

(a) All replicates of wildtype samples R^2=0.93 (b) All replicates of mutant samples R^2=0.92

Figure (8) Slope, correlation, LOD and LOQ determination using RSEM and STAR for all the wild type (a) mutant samples (b). Known concentrations are on the x-axis and observed concentration in TPMs is shown on the y-axis. Both the axes are log2 scaled. The vertical bar shows for each sequin isoforms shows the spread of the concentration values. No LOD or LOQ was detected for this sample set.

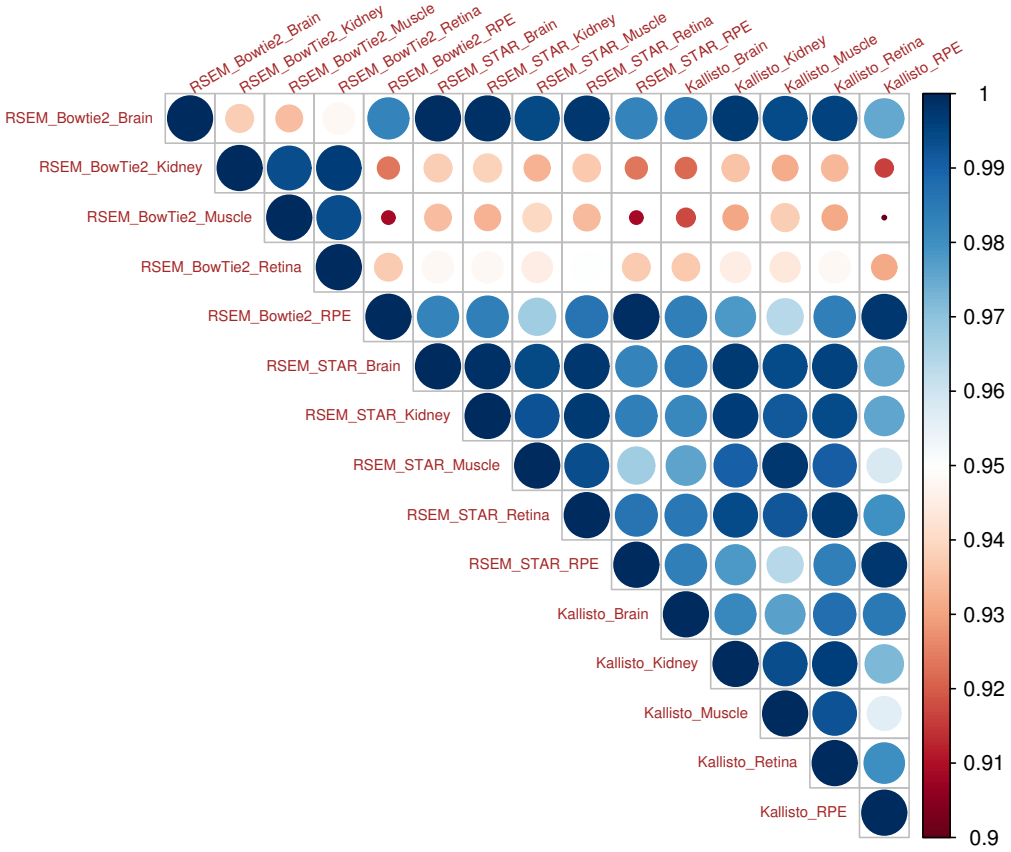

Figure (9) Correlation plot for comparative analysis for all the wild type samples using RSEM and two aligners along with Kallisto across all the mouse tissues. An upper triangular heatmap is generated showing Pearson correlation of determination values using average TPM expression values across the five mouse tissues. The combinations of tools used are shown in the format of:ExpressionTool_Aligner_Tissue,for example, RSEM_STAR_Brain. High correlation of determination values were observed across different tissues types and combinations of different tools. Similar observations were made for the mutant sample set, Supplementary Figure S10.

Differential Isoform Proportion and Expression

We investigated Differential Transcript Expression (DTE) proportions and directionality of LFC values across all the mouse tissues. As for DGE above, we expect the proportions of the LFC should be similar and unidirectional, provided that the depth of coverage and sequins ratios are proportional across the case and control samples. Supplementary Figure S12 shows proportions and directionality of sequins across all the mouse five tissues.

As with DGE, in most cases unified directionality and proportions of the isoforms was observed. The directionality and proportions of sequins with ground truth of zero LFC are over or under reported by one unit. Additionally, Supplementary Table S11 provides details on some of the specific sequins that were missed by either of both of the DTE tools. Overall, some inconsistencies in reporting of LFC proportions and directionality of the sequins were observed.

Supplementary Figure S11 shows an upper triangular computed correlation of determination in the form of a heatmap using complete case analysis approach. In this case, the missing values (sequins) were removed. The figure shows (R^2) values for all possible combinations for EBSeq and Sleuth across all the five mouse tissues. Here we followed the "complete case analysis"

Similar to DGE, we know underlying expected fold changes; up-regulation, down-regulation and no change (no LFC) of the sequin isoforms between the case and control sample sets across all the mouse tissues, we can gauge the sensitivity and specificity of various combinations of the tools using receiver operating characteristics (ROC) analysis. Figure 10 shows the ROC curve for all the mouse tissues with different combinations of all the analysis tools.

Each plot in the figure for a given tissue shows the performance of different combinations of the tools used for the alignments, isoform expression values and DTE. It is evident that the accuracy of isoform detection is not as good as for DGE. The shift in the curves for certain combinations of the tools was due to missed reporting of the sequin isoforms.

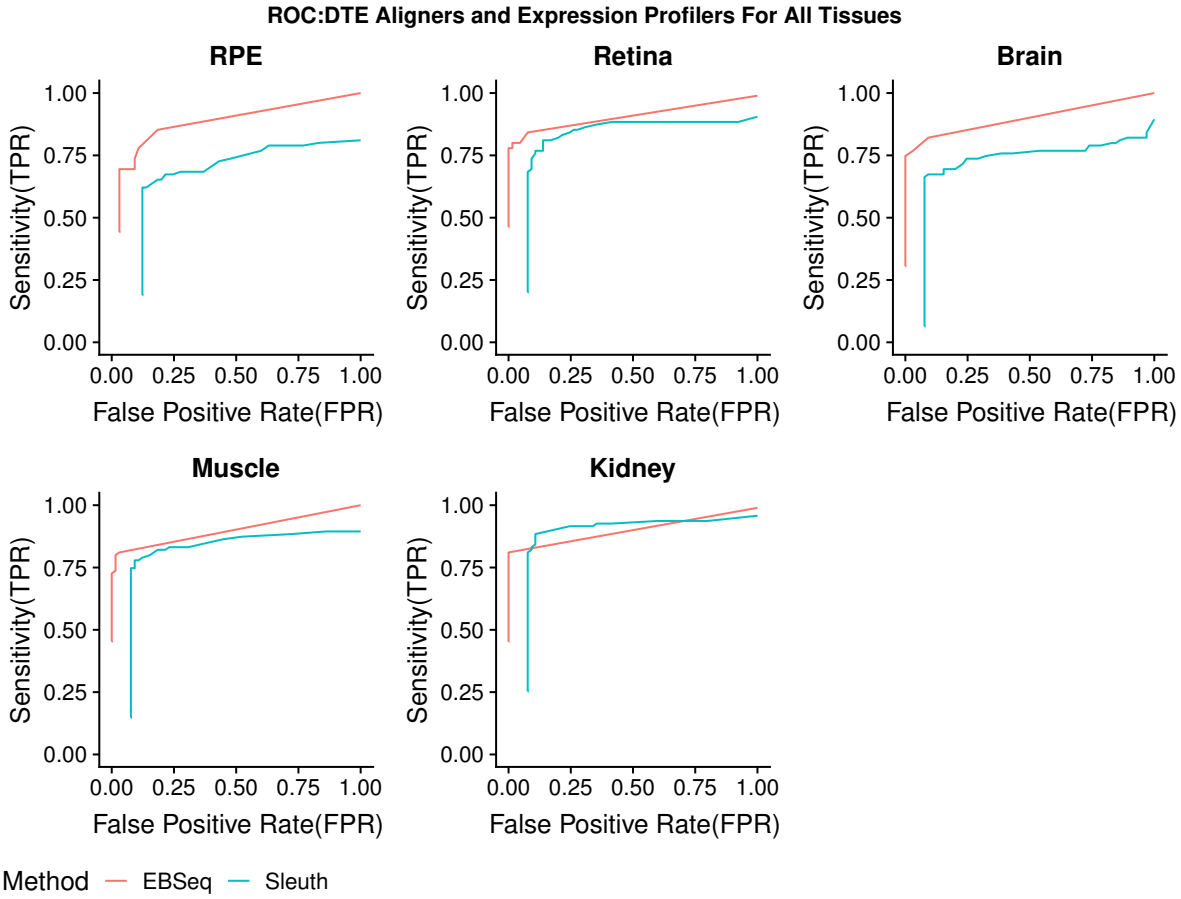

Figure (10) ROC (receiver operating characteristic) curves for Sequin isoforms for diagnostic performance in measuring fold change. Each plot reflects the performance of the aligners, feature read counting and DGE tools across all the five mouse tissues.

Differential Alternate Splicing

The sequins in each set of samples act as our truth set. Since the amount of each gene and isoform is known *a priori* we can use them for differential alternative splicing (AS) events detection across all the five mouse tissues. Our objective was to compare consistency and reproducibility of each of the splicing detection tools within the samples set and also across the tissue types. The RPE tissue was the first set of samples we used for comparative analysis for differential AS detection tools. Table 2 shows sensitivity for three tools. For RPE, JunctionSeq (86.3%) and MAJIQ (68.18%) outperformed rMATS (31%). Similarly, Table 3 shows specificity with JunctionSeq (97.87%) and MAJIQ (100%) outperforming rMATS(91.48%). We did not use rMATS for further analysis on other tissue types. With the exception of RPE, for the rest of the samples (retina, brain, kidney and muscle), observed sensitivity of JunctionSeq was 100%. MAJIQ showed lower sensitivity ranging from 59% to 90% (Table 2). MAJIQ showed a 100% specificity across all the tissues with JunctionSeq reporting at least one false positive except for the muscle tissue.

Table (2) Sequins sensitivity from differential splicing events tools. Calculated sensitivity across all the five mouse tissues is shown. rMATS was tested only on the RPE tissue types. Alignments were made using STAR.

Tool/ Tissue	**JunctionSeq**					**MAJIQ**					**rMATS**
	RPE	**Retina**	**Brain**	**Muscle**	**Kidney**	**RPE**	**Retina**	**Brain**	**Muscle**	**Kidney**	**RPE**
True Positive	19	22	22	22	22	15	19	13	17	20	7
False Negative	3	0	0	0	0	7	3	9	5	2	15
Sensitivity%	86.3	100	100	100	100	68.18	86.36	59.09	77.27	90.90	31.81

Table (3) Sequins specificity from differential splicing events tools. Calculated specificity across all the five mouse tissues is shown. rMATS was tested only on the RPE tissue types.

Tool/ Tissue	**JunctionSeq**					**MAJIQ**					**rMATS**
	RPE	**Retina**	**Brain**	**Muscle**	**Kidney**	**RPE**	**Retina**	**Brain**	**Muscle**	**Kidney**	**RPE**
True Negative	46	46	46	47	47	47	47	47	47	47	43
False Positive	1	1	1	0	0	0	0	0	0	0	4
Specificity%	97.87	97.87	97.87	100	100	100	100	100	100	90.90	91.48

Furthermore, Supplementary Table S12 shows comparative sensitivity from HISAT2 and STAR aligner. In both the case, MAJIQ was used for differential AS detection. HISAT2, in two cases; retina (90%) and brain (63%) slightly outperformed STAR aligner 86% and 59% respectively. In the rest of the samples/tissues, identical results were observed. No true negative was reported.

Additionally, we found comparable results in terms of sensitivity and specificity between the combination of JunctionSeq with STAR and JunctionSeq with HISAT2(Supplementary Table S13)

with two exceptions. The combination of HISAT2 and JunctionSeq for retina and muscle samples found to have higher reporting of false positives 5 and 2, respectively than the combination of STAR and JunctionSeq. Near identical sensitivity and specificity was observed the remaining tissue types.

Finally, recall that JunctionSeq is capable of identifying novel splice junctions. We analyzed novel splice junctions reported by JunctionSeq by the two aligners on sequins only. Any reported novel junctions are false positives. Supplementary Table S14 shows comparison of novel splice junction from the two aligners. No more than 3 novel splice junctions per gene was observed. We observed more novel splice junctions from the STAR aligner than HISAT2.

Impacts of Downsampling on Gene, Isoform and Splicing

We investigated the impacts of lower depth of coverage on detection of gene expression, DGE, isoform expression and DTE and AS events using sequins. We made three tiers of the aligned data set using 150 million, 100 million and 50 million sequence reads. In the previous sections we show that sensitivity and specificity of the aligners, genes and isoform expression profilers are comparable. We used the output from the STAR aligner, featureCount for gene expression profile and used DESeq2 for DGE. Similarly, we used Kallisto for isoform expression, Sleuth for DTE. MAJIQ was used for AS events. Supplementary Table S15, Table S16 and Table S17 show different metrics associated with downsampling for the RPE, retina and brain sample respectively. Various metrics such as, total genomics reads, genomics unique alignment counts, total sequins reads, expected and observed reads counts of sequins post downsampling is shown. Due to lower depth of coverage, two samples in the RPE sample set and one sample in the brain could not be downsampled to 150 million tier. Similarly, two samples in the RPE sample set could not be downsampled to 50 million tier, 5 samples for 100 million and 6 samples for 150 million tier could not downsampled. In all such case the entire sample set was used.

Genes

Figure 11 shows the correlation plots of the all three tiers for RPE data set. 2 true positive (TP) sequin was not reported in the 50 million set for RPE. No LOD and LOQ were reported from Anaquin for mouse RPE sample set. Similar observations were made for the retina and brain samples for the all the three tiers. 1 TP sequin was not reported in the 50 milllion set for retina and 1 TP sequins

in each of 150 million and 50 million was not reported in the brain tissue. High correlation was observed across between the expected and observed LFC for RPE, retina and brain.

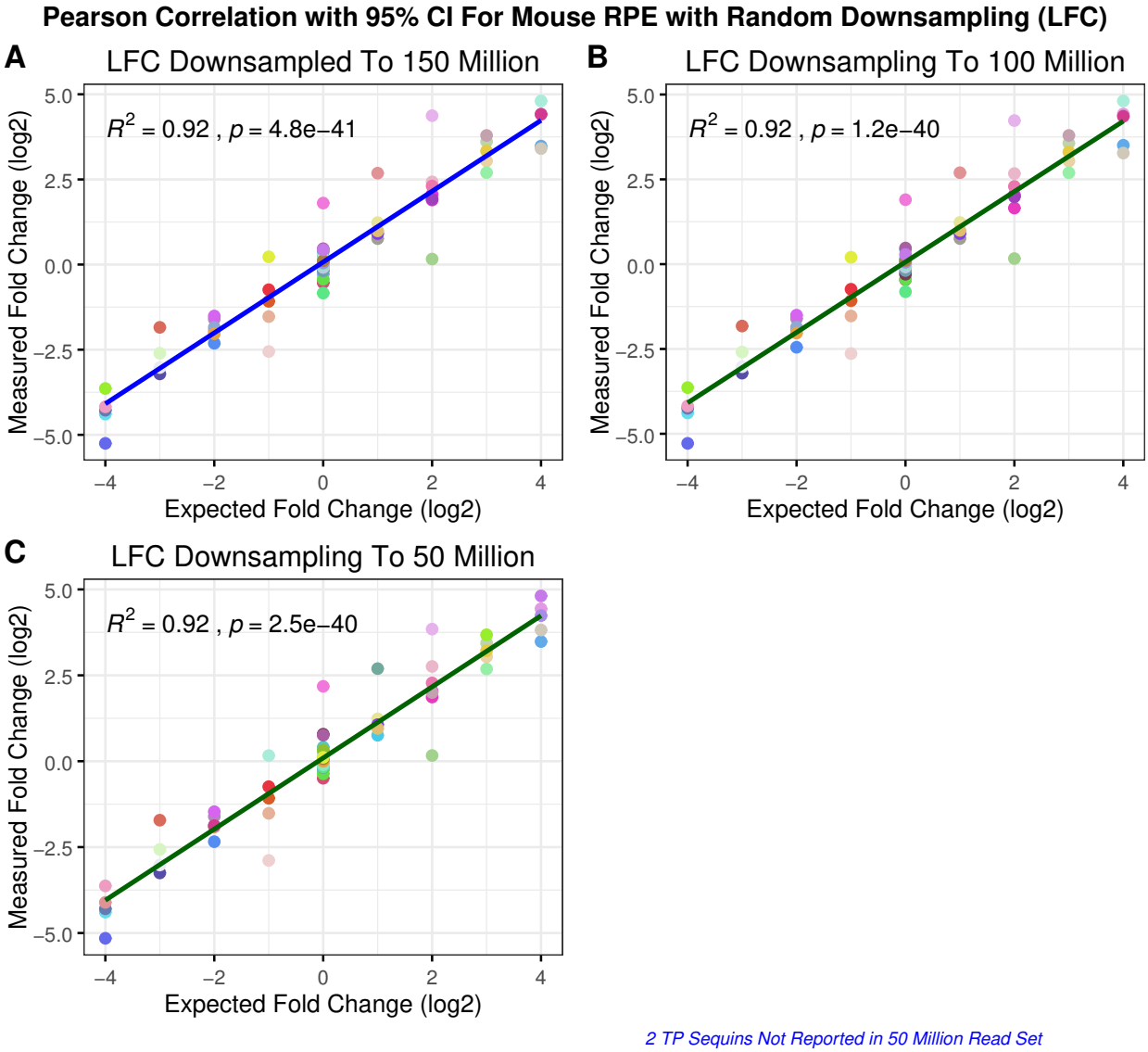

Figure (11) Correlation plot for comparative analysis for mouse RPE for downsampled data. The x-axis represents the expected LFC in log2 values and y-axis represents the observed LFC values by the differential gene expression tools. The plot of LFC for sequin genes across all the three titers is shown. Here we have used DESeq2 only. In the figure, each sequin gene is assigned a unique and static color across the different tissues. The Pearson correlation was calculated for each combinatorial methodology. As per the CI interval, there were some over and some under represented genes. Overall high correlation was observed. We did observed loss of 2 true positive sequins in the 50 million read set.

Next, as with original dataset, we focused on the correlation between the expected and observed LFC values, including the proportions and directionality. Supplementary Figure S13 shows comparison of proportions and directionality for all the three tissues and the three downsampling tiers. As with the complete dataset, some sequins (ranging of 1–2) were not reported. Sequins genes between -1

–+1 showed more variations than the other LFC values.

Isoforms

Next we explored impacts of lower DOC on the sequin isoforms. Figure12, shows correlation between the expected and observed expressions for mouse RPE, tissue with lowest DOC. Similar observations were made with the mutant replicates. No LOD or LOQ was detected for any of the three downsampled tiers and for all three tissues

Table4 summarizes the observed correlation of determination across brain and retina across the three tiers.

Table (4) Pearson correlation for downsampled isoforms from mouse retina and brain samples. Random down sampling was performed using different seeds.

ReadCnts/Tissue	150Million	100Million	50Million
Retina_WT	0.85	0.83	0.67
Retina_MUT	0.88	0.81	0.79
Brain_WT	0.78	0.72	0.83
Brain_MUT	0.70	0.64	0.62

Downsampling impacted the isoform LFC the most. No significant LFC sequins were reported for the brain and RPE tissues for all the three titration blocks. In the case of retina, for 100 million reads 6 TP sequins and 1 for the 50 million read set were reported. Similar to isoforms, reporting of AS events also was impacted.

The gene expression and DGE data set remains accurate when the RNA-Seq data are down-sampled. In contrast downsampling noticeability impacted isoform detection and DTE. We observed hight variability across replicates for all the three tiers of the dataset negatively impacting the correlation coefficient.

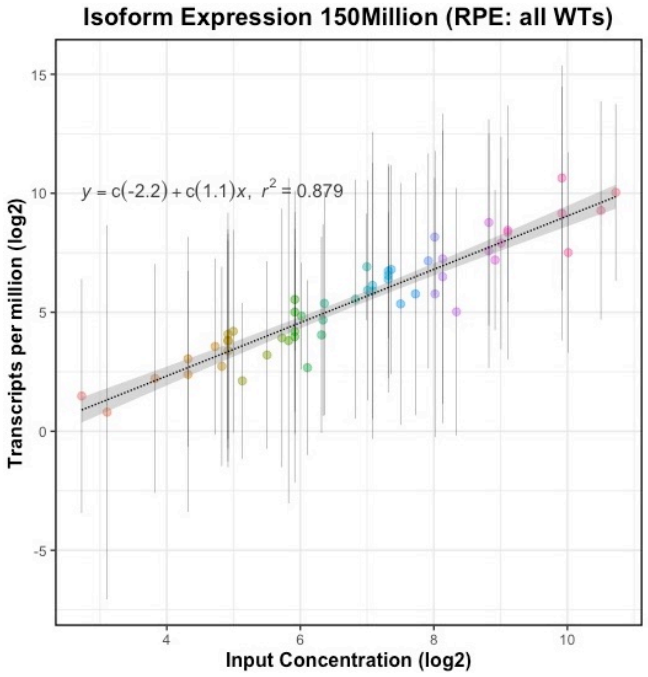

(a) RPE wild type 150 million set

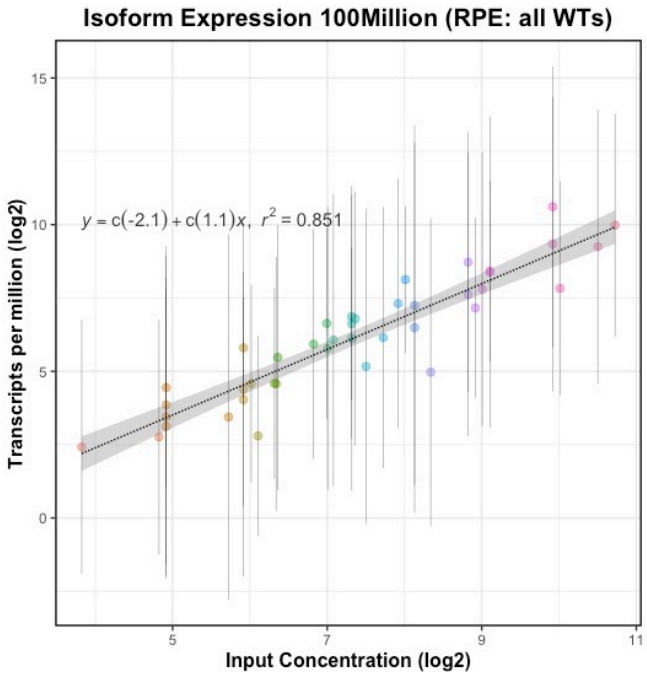

(b) RPE wild type 100 million set

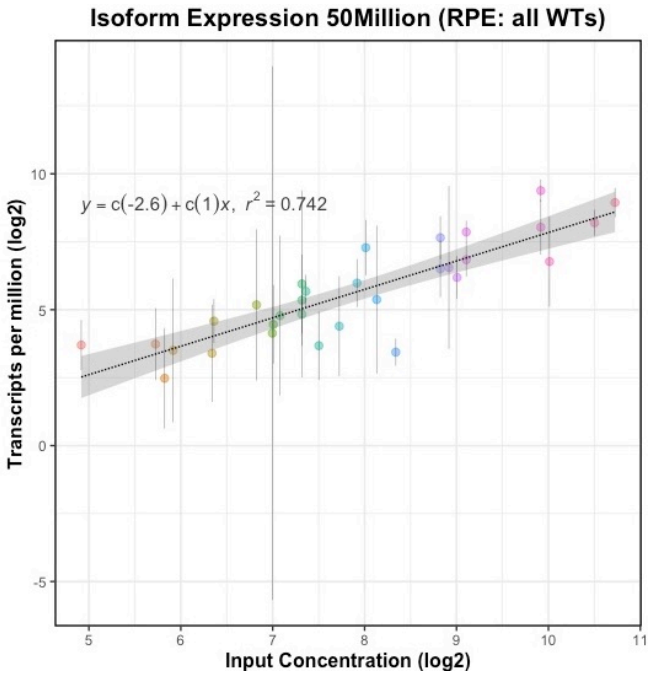

(c) RPE wild type 50 million set

Figure (12) Correlation plot for downsampled mouse RPE wild type (a) mutant tissues (b) for random 150 million reads. Slope, correlation, LOD and LOQ determination for Kallisto is shown. Known concentration are on the x-axis and observed concentration in TPMs is shown on the y-axis. Both the axis are log2 scaled. The vertical bar shows for each sequin isoforms shows the spread of the concentration values. No LOD or LOQ was detected for this sample set. Observed R^2=0.87 values for WT, R^2=0.91 for MUT

Splicing

Table 5 summarizes the sensitivity of the AS events from MAJIQ. No true negative was reported. For comparison, sensitivity from the original data is also listed. We observed decrease in sensitivity of differential AS detection with lower DOC.

Table (5) Sensitivity for detection of AS events on downsampled data. The three mouse tissues were downsampled into 3 tiers; 150, 100 and 50 million read set. MAJIQ was used for AS detection. The reads were aligned using STAR. No true negative was reported. The brain sample set is worst affected. Not that in true sense this is the sample set where each sample set underwent downsampling. In RPE and retina, there were many sample that were used entirely due to lack of read counts.

Tissue	**RPE**			**Retina**			**Brain**		
Read Cnts	**150Mill**	**100Mill**	**50Mill**	**150Mill**	**100Mill**	**50Mill**	**150Mill**	**100Mill**	**50Mill**
TP	15	14	13	19	16	15	12	11	9
FN	7	8	9	3	6	7	10	11	13
Sensitivity%	68.2	63.6	59.1	86.4	72.7	68.2	54.5	50.0	40.9
Orignal Sensitivity%	68.18			86.3			59.09		

Discussion

In this study we have evaluated the performance of different tools required to analyze the data from a typical RNA-Seq experiment. We added known mixtures of internal control “sequins” to RNA samples prior to library preparation and sequencing, allowing for quantification of the accuracy of the output from different software tools. Using this approach we demonstrate the use of these internal controls in a RNA-Seq work flow is vital for robust routine assessment of RNA-Seq experiments during experimental and computational development .

Two orthogonal mapping methods, HISAT2 and STAR were evaluated at various levels. We compared unique genomic alignment rate, alignment to synthetic chromosome and to known synthetic intron. In our case, comparable results from both the aligners was observed. We did not observed any preferential bias of one mapper over the other. The performance of the aligner are known to vary based on the genome complexity (different strain and species) [13] and [14]. Our focus remained on sequins validated human and mouse genomes. We did not focus on the run times and there are others studies that have explored this in more details [14] and [45]. Testing every parameter is beyond the scope of this paper. Please see [16] and [13] for more details.

The read count matrices were produced by two different tools, featureCount and HTSeq-Count.

This allowed us to perform an unbiased comparison of the features (exons) expression profiles (count matrix) using different combination of the aligners. We did not observed any change in behavior from the aligners or from the expression profile tools. Furthermore, no LOD/LOQ was reported regardless of the aligners, expression count matrix tool and tissue types across the two genotypes and replicates. Expected concentrations of all the genes, inclusive of lowly expressed genes was obtained. Comparable results were obtained from both the expression profilers [25], [23] and [45]. To observe the impacts of lower depth of coverage, we downsampled the original data into three (3) tiers of random read sets. Even with downsampled data, as low as 50 million reads consistent and robust correlation of determination was observed. In all the cases, sensitivity was impacted for genes with should have zero expression. We observed reporting of sequin genes expression in range of -1–+1 units. Such cases reflects both on the alignment, as the reads were aligned to such sequin in a disproportionate manner and further compounded by the expression profilers.

We analyzed DESeq2 and edgeR using different combination of the aligners and read count expression matrix tools. Since sequins were added to all the tissues, this analysis was not only performed in a typical form, that is restricted to within tissues and its corresponding genotypes. The analysis was extended across all the five tissues for comparative analysis. Systematic observations were made: high correlation of determination, consistent proportion and directionality across all the tissues and high sensitivity. We observed that DESeq2 does not report LFC values with low sensitivity, the same could not be said for edgeR. In internal testing, using a third highest LFC value cutoff for edgeR, both the DGE tools were indistinguishable. Both the tools were resilient to any negative impacts of lower depth of coverage. We observed high correlation of determination among the different tissues. For sequin genes which should be constant across the two genotype (sequins mixtures), LFC in range of -1–+1 was reported. In such cases the DGE tools were not able to normalize for disproportionate read alignment and expressions for such specific cases. Using sequins, one can determine the range of LFC that should not be considered and apply such filter to the genomic set to exclude such DGE genes from all downstream analysis.

We analyzed isoform expressions and differential expression using different combinations of the software packages. We used RSEM with Bowtie2 and STAR and another orthogonal software Kallisto for isoform expression within the two genotypes across the five tissues. High correlation was observed with different combination of RSEM and the two aligners. No LOD or LOQ was

reported. Similar observation was made with Kallisto. However, robustness of these tools was negatively impacted with lower DOC. We observed a decreasing trend in correlation of determination with corresponding lowering of DOC. Although, with lower DOC, no LOD or LOQ was reported, but extreme variability across the replicates for the sequin isoforms was observed, most with 50 million downsampled dataset. For isoform detection high DOC (>150 million HQ reads) is needed.

EBSeq and Slueth were used for LFC. Combination for RSEM and EBSeq and Kallisto with Sleuth was used. We found irregularities in the reporting of the sequins and their predicted proportions and directionality by both the tools. In almost all the tissues high up-regulated and down-regulated isoforms were reported consistently. The lower expressing sequin isoforms in the range of -1–+1 including isoforms with no (zero) LFC were missed or if reported, inconsistencies in the proportions were observed. DTE tools were intolerant to lower DOC. Insignificant number of true positive sequin isoforms with confidence were reported by the DTE tools. As with isoform expression, caution is advised for DTE with DOC of 150 million reads. The DTE tools were not found as robust and refined as the DGE tools.

We used count-based methods that include both exon-based and event-based approaches; rMATS, MAJIQ and JunctionSeq. We tested alignment from both STAR and HISAT2. The mouse RPE tissue had the lowest depth of coverage compared to other tissues. We first used this tissue to identify best AS tools. MAJIQ and JunctionSeq outperformed rMATS. We next tested and compared MAJIQ and JunctionSeq with rest of the tissues for consistency and reproducibility. Minimal (1) false positives were reported by MAJIQ or JunctionSeq. In most cases with regards to sensitivity and specificity JunctionSeq was found outperforming MAJIQ. In three cases, RPE, retina and brain, JunctionSeq reported one false positive, none was reported by MAJIQ.

Since absence of reporting of AS events in classical sense, we found it hard to interpret the observed phenomenas from JunctionSeq used as a proxy to AS or convert the output to be more interpretable compared to MAJIQ. Even though JunctionSeq produces a number of images for DEU, we found that output from MAJIQ's companion tool "Volia" was easier to interpret. With such a high depth of coverage we find it disconcerting that not all the true positive sequins were reported by MAJIQ. Lower depth of coverage impacted sensitivity to predict AS events of known true positive events. A decreasing trend is the sensitivity across three tiers of downsampling and three tissue was observed. No true negative event was reported.

We used sequins as ground truth for systematic evaluate different tools used during RNA-Seq analysis. We demonstrated that inclusion of internal controls in RNA-seq experiments allows accurate determination of detection levels, and better assessment of DGE, DTE and AS accuracy. The gene expression profiling and DGE tools are found to be robust. The isoform expression profiling tools were robust, but not as tolerant to lower depth of coverage as the DGE tools. We recommend high depth of coverage, about 200 million reads for confident prediction of differential isoform expression. Even with high DOC, for AS event detection, we found the current tools lacking high sensitivity. This was compounded by lower depth of coverage. More efforts are needed to improve specificity and sensitivity of DTE and AS detection.

References

[1] Valerio Costa, Marianna Aprile, Roberta Esposito, and Alfredo Ciccodicola. Rna-seq and human complex diseases: recent accomplishments and future perspectives. *European Journal of Human Genetics*, 21(2):134–142, 2013.

[2] Chiara Di Resta, Silvia Galbiati, Paola Carrera, and Maurizio Ferrari. Next-generation sequencing approach for the diagnosis of human diseases: open challenges and new opportunities. *Ejifcc*, 29(1):4, 2018.

[3] Amelia Casamassimi, Antonio Federico, Monica Rienzo, Sabrina Esposito, and Alfredo Ciccodicola. Transcriptome profiling in human diseases: new advances and perspectives. *International journal of molecular sciences*, 18(8):1652, 2017.

[4] Isabelle Audo, Kinga M Bujakowska, Thierry Léveillard, Saddek Mohand-Saïd, Marie-Elise Lancelot, Aurore Germain, Aline Antonio, Christelle Michiels, Jean-Paul Saraiva, Mélanie Letexier, et al. Development and application of a next-generation-sequencing (ngs) approach to detect known and novel gene defects underlying retinal diseases. *Orphanet journal of rare diseases*, 7(1):8, 2012.

[5] Kasper Lage, Niclas Tue Hansen, E Olof Karlberg, Aron C Eklund, Francisco S Roque, Patricia K Donahoe, Zoltan Szallasi, Thomas Skøt Jensen, and Søren Brunak. A large-scale analysis of tissue-specific pathology and gene expression of human disease genes and complexes. *Proceedings of the National Academy of Sciences*, 105(52):20870–20875, 2008.

[6] Dirk A Kleinjan and Veronica van Heyningen. Long-range control of gene expression: emerging mechanisms and disruption in disease. *The American Journal of Human Genetics*, 76(1):8–32, 2005.

[7] Juliana Costa-Silva, Douglas Domingues, and Fabricio Martins Lopes. Rna-seq differential expression analysis: An extended review and a software tool. *PloS one*, 12(12):e0190152, 2017.

[8] Amanda J Ward and Thomas A Cooper. The pathobiology of splicing. *The Journal of Pathology: A Journal of the Pathological Society of Great Britain and Ireland*, 220(2):152–163, 2010.

[9] Nicole Weisschuh, Elena Buena-Atienza, and Bernd Wissinger. Splicing mutations in inherited retinal diseases. *Progress in retinal and eye research*, page 100874, 2020.

[10] Eddie Park, Zhicheng Pan, Zijun Zhang, Lan Lin, and Yi Xing. The expanding landscape of alternative splicing variation in human populations. *The American Journal of Human Genetics*, 102(1):11–26, 2018.

[11] Mihaela Pertea, Geo M Pertea, Corina M Antonescu, Tsung-Cheng Chang, Joshua T Mendell, and Steven L Salzberg. Stringtie enables improved reconstruction of a transcriptome from rna-seq reads. *Nature biotechnology*, 33(3):290, 2015.

[12] Charlotte Soneson, Michael I Love, and Mark D Robinson. Differential analyses for rna-seq: transcript-level estimates improve gene-level inferences. *F1000Research*, 4, 2015.

[13] Giacomo Baruzzo, Katharina E Hayer, Eun Ji Kim, Barbara Di Camillo, Garret A FitzGerald, and Gregory R Grant. Simulation-based comprehensive benchmarking of rna-seq aligners. *Nature methods*, 14(2):135, 2017.

[14] Sayed Mohammad Ebrahim Sahraeian, Marghoob Mohiyuddin, Robert Sebra, Hagen Tilgner, Pegah T Afshar, Kin Fai Au, Narges Bani Asadi, Mark B Gerstein, Wing Hung Wong, Michael P Snyder, et al. Gaining comprehensive biological insight into the transcriptome by performing a broad-spectrum rna-seq analysis. *Nature communications*, 8(1):1–15, 2017.

[15] Arfa Mehmood, Asta Laiho, Mikko S Venäläinen, Aidan J McGlinchey, Ning Wang, and Laura L Elo. Systematic evaluation of differential splicing tools for rna-seq studies. *Briefings in Bioinformatics*, 2019.

[16] Sara Ballouz, Alexander Dobin, Thomas R Gingeras, and Jesse Gillis. The fractured landscape of rna-seq alignment: the default in our stars. *Nucleic acids research*, 46(10):5125–5138, 2018.

[17] Harold Pimentel, Nicolas L Bray, Suzette Puente, Páll Melsted, and Lior Pachter. Differential analysis of rna-seq incorporating quantification uncertainty. *Nature methods*, 14(7):687, 2017.

[18] Shawn C Baker, Steven R Bauer, Richard P Beyer, James D Brenton, Bud Bromley, John Burrill, Helen Causton, Michael P Conley, Rosalie Elespuru, Michael Fero, et al. The external rna controls consortium: a progress report. *Nature methods*, 2(10):731, 2005.

[19] Chi Zhang, Baohong Zhang, Lih-Ling Lin, and Shanrong Zhao. Evaluation and comparison of computational tools for rna-seq isoform quantification. *BMC genomics*, 18(1):583, 2017.

[20] Zhenqiang Su, Paweł P Łabaj, Sheng Li, Jean Thierry-Mieg, Danielle Thierry-Mieg, Wei Shi, Charles Wang, Gary P Schroth, Robert A Setterquist, John F Thompson, et al. A comprehensive assessment of rna-seq accuracy, reproducibility and information content by the sequencing quality control consortium. *Nature biotechnology*, 32(9):903–914, 2014.

[21] Lichun Jiang, Felix Schlesinger, Carrie A Davis, Yu Zhang, Renhua Li, Marc Salit, Thomas R Gingeras, and Brian Oliver. Synthetic spike-in standards for rna-seq experiments. *Genome research*, 21(9):1543–1551, 2011.

[22] Simon A Hardwick, Wendy Y Chen, Ted Wong, Ira W Deveson, James Blackburn, Stacey B Andersen, Lars K Nielsen, John S Mattick, and Tim R Mercer. Spliced synthetic genes as internal controls in rna sequencing experiments. *Nature methods*, 13(9):792, 2016.

[23] Alexander Dobin, Carrie A Davis, Felix Schlesinger, Jorg Drenkow, Chris Zaleski, Sonali Jha, Philippe Batut, Mark Chaisson, and Thomas R Gingeras. Star: ultrafast universal rna-seq aligner. *Bioinformatics*, 29(1):15–21, 2013.

[24] Daehwan Kim, Ben Langmead, and Steven L Salzberg. Hisat: a fast spliced aligner with low memory requirements. *Nature methods*, 12(4):357, 2015.

[25] Yang Liao, Gordon K Smyth, and Wei Shi. featurecounts: an efficient general purpose program for assigning sequence reads to genomic features. *Bioinformatics*, 30(7):923–930, 2013.

[26] Simon Anders, Paul Theodor Pyl, and Wolfgang Huber. Htseq—a python framework to work with high-throughput sequencing data. *Bioinformatics*, 31(2):166–169, 2015.

[27] Michael I Love, Wolfgang Huber, and Simon Anders. Moderated estimation of fold change and dispersion for rna-seq data with deseq2. *Genome biology*, 15(12):550, 2014.

[28] Mark D Robinson, Davis J McCarthy, and Gordon K Smyth. edger: a bioconductor package for differential expression analysis of digital gene expression data. *Bioinformatics*, 26(1):139–140, 2010.

[29] Bo Li and Colin N Dewey. Rsem: accurate transcript quantification from rna-seq data with or without a reference genome. *BMC bioinformatics*, 12(1):1, 2011.

[30] Nicolas L Bray, Harold Pimentel, Páll Melsted, and Lior Pachter. Near-optimal probabilistic rna-seq quantification. *Nature biotechnology*, 34(5):525, 2016.

[31] Ning Leng, John A Dawson, James A Thomson, Victor Ruotti, Anna I Rissman, Bart MG Smits, Jill D Haag, Michael N Gould, Ron M Stewart, and Christina Kendziorski. Ebseq: an empirical bayes hierarchical model for inference in rna-seq experiments. *Bioinformatics*, 29(8):1035–1043, 2013.

[32] Stephen W Hartley and James C Mullikin. Detection and visualization of differential splicing in rna-seq data with junctionseq. *Nucleic acids research*, 44(15):e127–e127, 2016.

[33] Jorge Vaquero-Garcia, Alejandro Barrera, Matthew R Gazzara, Juan Gonzalez-Vallinas, Nicholas F Lahens, John B Hogenesch, Kristen W Lynch, and Yoseph Barash. A new view of transcriptome complexity and regulation through the lens of local splicing variations. *elife*, 5:e11752, 2016.

[34] Kinga Bujakowska, Cecilia Maubaret, Christina F Chakarova, Naoyuki Tanimoto, Susanne C Beck, Edda Fahl, Marian M Humphries, Paul F Kenna, Evgeny Makarov, Olga Makarova, et al. Study of gene-targeted mouse models of splicing factor gene prpf31 implicated in human autosomal dominant retinitis pigmentosa (rp). *Investigative ophthalmology & visual science*, 50(12):5927–5933, 2009.

[35] Eranga N Vithana, Leen Abu-Safieh, Maxine J Allen, Alisoun Carey, Myrto Papaioannou, Christina Chakarova, Mai Al-Maghtheh, Neil D Ebenezer, Catherine Willis, Anthony T Moore, et al. A human homolog of yeast pre-mrna splicing gene, prp31, underlies autosomal dominant retinitis pigmentosa on chromosome 19q13. 4 (rp11). *Molecular cell*, 8(2):375–381, 2001.

[36] Rosario Fernandez-Godino, Donita L Garland, and Eric A Pierce. Isolation, culture and characterization of primary mouse rpe cells. *Nature protocols*, 11(7):1206–1218, 2016.

[37] Babraham Bioinformatics. Fastqc a quality control tool for high throughput sequence data. *Cambridge, UK: Babraham Institute*, 2011.

[38] Philip Ewels, Måns Magnusson, Sverker Lundin, and Max Käller. Multiqc: summarize analysis results for multiple tools and samples in a single report. *Bioinformatics*, 32(19):3047–3048, 2016.

[39] Ben Langmead and Steven L Salzberg. Fast gapped-read alignment with bowtie 2. *Nature methods*, 9(4):357, 2012.

[40] Heng Li, Bob Handsaker, Alec Wysoker, Tim Fennell, Jue Ruan, Nils Homer, Gabor Marth, Goncalo Abecasis, and Richard Durbin. The sequence alignment/map format and samtools. *Bioinformatics*, 25(16):2078–2079, 2009.

[41] Taiyun Wei, Viliam Simko, Michael Levy, Yihui Xie, Yan Jin, and Jeff Zemla. Package 'corrplot'. *Statistician*, 56(316):e24, 2017.

[42] Shihao Shen, Juw Won Park, Zhi-xiang Lu, Lan Lin, Michael D Henry, Ying Nian Wu, Qing Zhou, and Yi Xing. rmats: robust and flexible detection of differential alternative splicing from replicate rna-seq data. *Proceedings of the National Academy of Sciences*, 111(51):E5593–E5601, 2014.

[43] Michael H Farkas, Deborah S Lew, Maria E Sousa, Kinga Bujakowska, Jonathan Chatagnon, Shomi S Bhattacharya, Eric A Pierce, and Emeline F Nandrot. Mutations in pre-mrna processing factors 3, 8, and 31 cause dysfunction of the retinal pigment epithelium. *The American journal of pathology*, 184(10):2641–2652, 2014.

[44] Ted Wong, Ira W Deveson, Simon A Hardwick, and Tim R Mercer. Anaquin: a software toolkit for the analysis of spike-in controls for next generation sequencing. *Bioinformatics*, 33(11):1723–1724, 2017.

[45] Pierre-Luc Germain, Alessandro Vitriolo, Antonio Adamo, Pasquale Laise, Vivek Das, and Giuseppe Testa. Rnaonthebench: computational and empirical resources for benchmarking

rnaseq quantification and differential expression methods. *Nucleic acids research*, 44(11):5054–5067, 2016.

Supplementary Material

Table (S1) Genomes and versions. Table lists all the genomes and corresponding versions used in the analysis.

Reference	**Version**
Mouse Genome	MM10
Mouse GENCODE Gene Model	M12 (Ensembl 87)
Mouse rRNA NCBI	Nucleotide: txid10090

Table (S2) Analysis tools and versions. Table lists all the analysis tools that were used during the analysis.

Software	**Version**
FastQC	0.11.3
MultiQC	1.2
STAR	2.5.3a
HISAT2	2.1.0
rMATS (turbo)	4.0.2
MAJIQ	1.1.5
SubRead	1.5.2
HTSeq	0.9.1
RSeQC	2.6.4
edgeR	3.22.2
DESeq2	1.20.0
SmartSVA	0.1.3
SVA	0.1.3
Samtools	1.4
BowTie2	2.2.4
Picardtools	1.87
Anaquin	2.4.0
RStudio	1.1.453
R	3.5.0
Corrplot	0.85

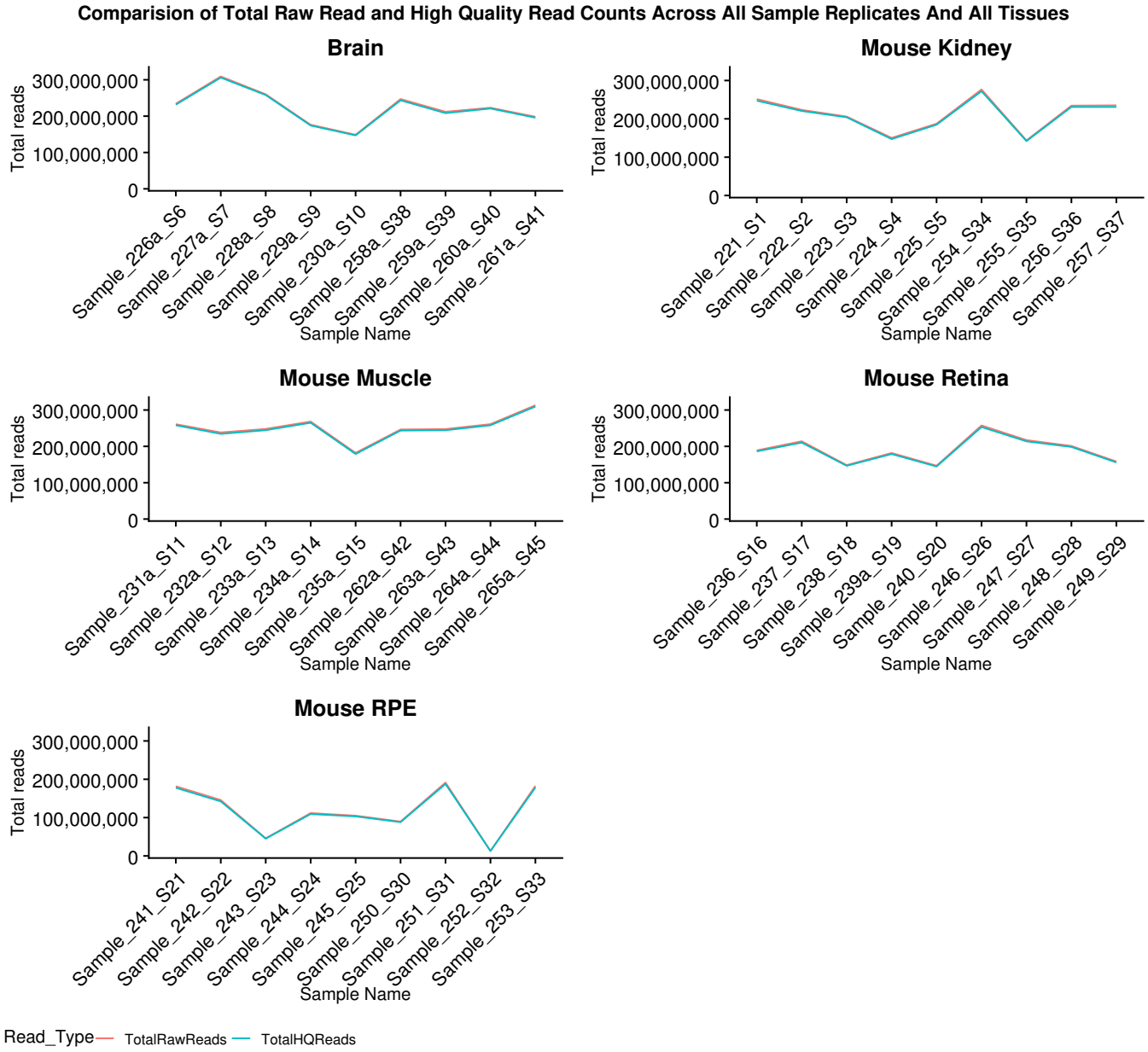

Figure (S1) Total read comparative pre and post processing. The figure shows total raw reads for each sample replicates including reads counts post quality processing. Total reads retained post QC ranged from 98%-99%, reflective in indistinguishable trend lines. The muscle and brain sample sets were among the highest read counts and as expected the RPE sample set showed the lowest read counts. For visualization only, discrete data is shown in a continuous form. From left to right, first 5 are mutants followed by wild type samples. HQ refers to reads and bases that have passed strict QC/QA processes.

Table (S3) Summary statistics of the first sequencing run. Table lists various standard summary statistics. RC refers to read counts and SRun refers to sequencing run.

Tissue	Min_RC	Max_RC	Mean	q1	q3	sstdev	SRun
Brain_MUT	17,774,374.00	47,831,123.00	32,978,284.80	30,247,107.00	38,115,267.00	11,066,114.35	180316_SideA
Brain_WT	44,964,350.00	53,334,326.00	49,872,655.25	48,962,570.75	51,506,057.00	3,526,178.06	180316_SideA
Kidney_MUT	18,908,291.00	61,991,216.00	40,235,123.20	33,223,708.00	47,277,456.00	16,024,415.00	180316_SideA
Kidney_WT	29,640,312.00	50,646,709.00	38,913,504.75	34,499,694.00	42,097,309.75	8,785,940.94	180316_SideA
Muscle_MUT	33,060,197.00	64,369,275.00	49,152,008.00	45,138,649.00	56,726,582.00	11,950,010.66	180316_SideA
Muscle_WT	38,495,751.00	79,720,781.00	58,744,616.50	47,683,314.00	69,442,269.50	17,952,446.39	180316_SideA
RPE_MUT	10,155,891.00	26,240,789.00	20,287,271.80	18,934,136.00	25,800,007.00	6,525,159.07	180316_SideA
RPE_WT	2,322,331.00	53,878,507.00	29,086,839.00	13,988,974.75	45,171,123.25	23,312,138.81	180316_SideA
Retina_MUT	29,616,145.00	53,113,782.00	39,190,498.00	32,174,368.00	45,054,179.00	9,738,485.57	180316_SideA
Retina_WT	22,053,007.00	45,558,421.00	34,166,835.00	29,885,213.50	38,809,577.50	9,747,341.21	180316_SideA

Table (S4) Summary statistics of the second sequencing run. Table lists various standard summary statistics. RC refers to read counts and SRun refers to sequencing run.

Tissue	Min_RC	Max_RC	Mean	q1	q3	sstdev	SRun
Brain_MUT	32,152,639.00	72,220,552.00	48,857,344.80	38,315,775.00	54,289,238.00	15,555,671.49	180329_SideB
Brain_WT	29,380,289.00	50,532,898.00	41,078,208.50	33,540,529.25	49,737,502.75	10,559,804.43	180329_SideB
Kidney_MUT	29,168,341.00	48,734,586.00	41,962,012.20	39,821,176.00	47,259,649.00	7,911,986.32	180329_SideB
Kindey_WT	30,573,417.00	56,677,704.00	49,143,940.50	48,246,328.50	55,559,932.50	12,424,146.74	180329_SideB
Muscle_MUT	39,911,361.00	55,456,660.00	48,490,047.20	46,087,495.00	52,144,800.00	5,945,303.49	180329_SideB
Muscle_WT	48,308,605.00	72,138,103.00	55,958,736.00	49,415,781.25	58,237,072.75	11,014,551.57	180329_SideB
RPE_MUT	8,690,207.00	40,478,959.00	25,355,064.40	20,918,726.00	34,186,494.00	12,372,054.76	180329_SideB
RPE_WT	2,691,785.00	37,939,584.00	23,939,273.00	14,265,830.00	37,236,304.50	16,851,461.92	180329_SideB
Retina_MUT	19,429,820.00	45,695,610.00	31,733,182.80	25,549,296.00	34,967,584.00	9,958,527.80	180329_SideB
Retina_WT	30,775,728.00	53,812,548.00	45,462,640.50	43,368,478.50	50,725,305.00	10,128,737.42	180329_SideB

Table (S5) Summary statistics of the third sequencing run. Table lists various standard summary statistics. RC refers to read counts and SRun refers to sequencing run.

Tissue	Min_RC	Max_RC	Mean	q1	q3	sstdev	SRun
Brain_MUT	31,206,610.00	71,171,799.00	47,950,791.80	37,449,205.00	53,467,718.00	15,512,327.00	180329_SideA
Brain_WT	29,320,150.00	50,315,623.00	41,006,583.00	33,579,969.25	49,621,893.25	10,481,788.24	180329_SideA
Kidney_MUT	28,445,740.00	47,628,004.00	40,863,701.00	38,879,103.00	45,994,335.00	7,689,469.31	180329_SideA
Kindey_WT	30,546,475.00	57,095,403.00	49,444,871.75	48,585,307.00	55,928,369.25	12,640,940.21	180329_SideA
Muscle_MUT	39,347,272.00	54,632,950.00	47,661,821.40	44,729,818.00	51,420,202.00	5,931,226.02	180329_SideA
Muscle_WT	48,814,196.00	72,757,284.00	56,667,476.00	50,124,164.00	59,092,524.00	10,990,655.58	180329_SideA
RPE_MUT	8,786,767.00	40,867,918.00	25,583,802.20	20,825,853.00	34,716,199.00	12,549,618.35	180329_SideA
RPE_WT	2,700,765.00	37,892,173.00	23,919,351.50	14,302,601.25	37,158,984.25	16,806,752.10	180329_SideA
Retina_MUT	19,472,261.00	45,802,587.00	31,750,870.20	25,560,530.00	34,968,562.00	9,979,074.85	180329_SideA
Retina_WT	30,768,953.00	54,046,702.00	45,746,491.00	43,761,905.75	51,069,739.75	10,287,252.19	180329_SideA

Table (S6) Summary statistics of the fourth sequencing run. Table lists various standard summary statistics. RC refers to read counts and SRun refers to sequencing run.

Tissue	Min_RC	Max_RC	Mean	q1	q3	sstdev	SRun
Brain_MUT	27,575,093.00	63,976,417.00	48,166,448.40	35,337,636.00	61,440,168.00	16,074,312.89	180420_SideB
Brain_WT	36,470,873.00	50,193,507.00	43,581,499.50	41,881,761.50	45,530,547.00	5,610,889.88	180420_SideB
Kidney_MUT	33,457,303.00	48,259,293.00	40,589,584.20	37,066,118.00	43,924,826.00	5,773,960.14	180420_SideB
Kidney_WT	23,225,180.00	66,183,582.00	42,328,409.75	33,320,651.00	48,960,197.25	17,950,254.02	180420_SideB
Muscle_MUT	29,438,918.00	57,359,123.00	47,734,526.00	48,031,299.00	52,781,014.00	10,770,227.19	180420_SideB
Muscle_WT	41,873,226.00	50,643,895.00	47,418,327.75	45,894,790.50	50,101,632.25	3,976,962.41	180420_SideB
RPE_MUT	9,074,588.00	37,295,963.00	23,545,374.60	22,435,199.00	25,669,359.00	10,053,759.91	180420_SideB
RPE_WT	2,631,976.00	36,212,909.00	20,968,421.75	14,082,932.50	29,399,890.25	14,329,301.50	180420_SideB
Retina_MUT	29,473,722.00	45,367,879.00	36,814,789.00	30,069,562.00	39,958,973.00	6,858,170.49	180420_SideB
Retina_WT	25,721,447.00	62,597,155.00	41,684,266.50	32,352,273.50	48,541,225.00	15,786,021.55	180420_SideB

Table (S7) Summary statistics of the fifth sequencing run. Table lists various standard summary statistics. RC refers to read counts and SRun refers to sequencing run.

Tissue	Min_RC	Max_RC	Mean	q1	q3	sstdev	SRun
Brain_MUT	26,876,041.00	63,668,498.00	47,740,737.40	34,978,434.00	61,202,734.00	16,210,221.15	180420_SideA
Brain_WT	36,918,458.00	51,027,046.00	44,568,074.25	43,034,603.00	46,696,867.75	5,801,149.03	180420_SideA
Kidney_MUT	32,463,591.00	47,972,862.00	40,001,739.60	36,662,935.00	43,323,351.00	5,973,191.54	180420_SideA
Kidney_WT	23,221,786.00	66,953,762.00	42,621,368.75	33,643,813.75	49,132,518.50	18,248,506.12	180420_SideA
Muscle_MUT	28,622,627.00	55,655,034.00	46,419,083.40	46,707,669.00	51,558,077.00	10,468,099.28	180420_SideA
Muscle_WT	42,425,732.00	51,545,746.00	48,249,609.75	46,647,989.75	51,115,100.50	4,172,479.27	180420_SideA
RPE_MUT	9,044,078.00	36,818,958.00	23,236,333.40	21,887,215.00	25,449,486.00	9,908,212.38	180420_SideA
RPE_WT	2,672,613.00	37,131,206.00	21,277,501.50	13,818,348.75	30,112,246.25	14,761,265.52	180420_SideA
Retina_MUT	29,204,397.00	44,957,206.00	36,465,152.40	29,553,853.00	39,923,484.00	6,882,867.79	180420_SideA
Retina_WT	25,431,971.00	62,675,224.00	41,452,999.50	32,082,930.50	48,222,470.50	15,937,718.54	180420_SideA

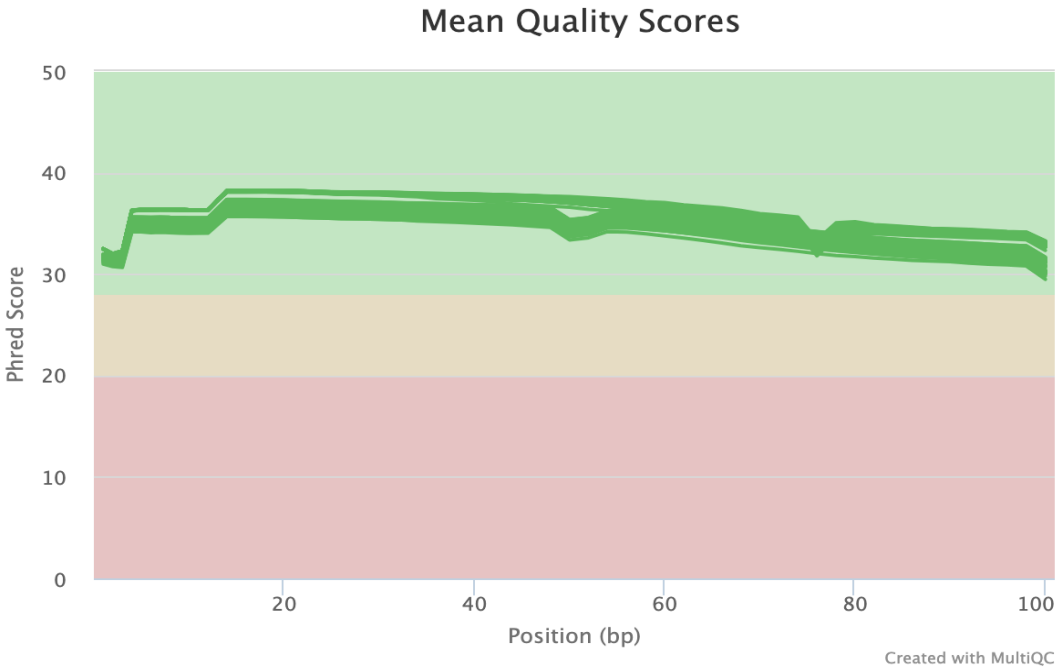

Figure (S2) Comparison of total reads of all the 45 samples. High mean phred quality per base, per cycle for the entire read length was observed. No biases were observed.

Table (S8) Sequins for differential genes expression. In the table all the true positive genes from the two mixtures are shown in attomoles/μl units, sorted from minimum-maximum. The genes cover true positive (TP), upregulation, downregulation and uniform (no change) set of sequins in the data set. There are 76 sequins genes for DGE.

ID	MixA	MixB	ID	MixA	MixB
R1_51	0.059	0.059	R2_63	1.8883	1.8883
R2_76	0.059	0.059	R2_73	1.8883	3.7766
R2_33	0.059	0.118	R1_11	1933.59	1933.59
R1_24	0.059	0.236	R2_154	1933.59	1933.59
R1_21	0.059	0.4721	R2_72	1933.59	1933.59
R2_105	0.118	0.059	R1_31	241.699	241.699
R1_93	0.118	0.118	R2_46	241.699	241.699
R2_152	0.118	0.118	R1_73	241.699	483.398
R2_47	0.118	0.118	R2_41	241.699	60.4248
R2_115	0.118	0.236	R1_91	30.2124	120.85
R1_53	0.236	0.059	R2_32	30.2124	15.1062
R2_37	0.236	0.059	R1_23	30.2124	30.2124
R1_63	0.236	0.236	R1_71	30.2124	30.2124
R2_54	0.236	0.236	R2_116	3.73883	3.73883
R1_82	0.236	1.8883	R2_68	3.7766	0.236
R1_42	0.4721	0.4721	R1_62	3.7766	0.9441
R1_81	0.4721	0.4721	R2_67	3.7766	15.1062
R2_20	0.4721	1.8883	R2_71	3.7766	3.7766
R1_12	0.4721	7.5531	R2_6	483.398	241.699
R2_143	0.4721	7.5531	R1_22	483.398	30.2124
R2_153	0.9441	0.4721	R2_38	483.398	483.398
R1_83	0.9441	0.9441	R2_42	483.398	483.398
R2_1	0.9441	0.9441	R1_14	483.398	966.797
R1_52	0.9441	15.1062	R2_140	60.4248	30.2124
R1_43	0.9441	7.5531	R1_32	60.4248	3.7766
R1_33	120.85	120.85	R2_117	60.4248	60.4248
R1_41	120.85	241.699	R2_28	60.4248	60.4248
R1_92	120.85	30.2124	R2_26	60.4248	7.5531
R1_13	120.85	483.398	R2_27	7.5531	0.9441
R2_53	120.85	966.797	R2_57	7.5531	0.9441
R2_24	15.1062	15.1062	R2_59	7.5531	120.85
R2_45	15.1062	15.1062	R2_60	7.5531	120.85
R1_101	15.1062	1.8883	R1_61	7.5531	7.5531
R2_19	15.1062	3.7766	R2_150	966.797	120.85
R1_102	15.1062	60.4248	R1_103	966.797	483.398
R1_72	1.8883	0.118	R2_7	966.797	60.4248
R2_55	1.8883	0.4721	R2_14	966.797	966.797
R2_151	1.8883	1.8883	R2_65	966.797	966.797

Table (S9) Sequins for differential isoform expression. In the table TP isoforms of the two mixtures (in attomoles/μl units) along with the length are shown, sorted from minimum-maximum of their respective concentration. The isoforms cover upregulation, downregulation and uniform (no change) set of sequins in the data set. There are 160 sequins isoform counts.

ID	Length	MixA	MixB	ID	Length	MixA	MixB	ID	Length	MixA	MixB
R1_21_2	794	0.0036875	0.44259375	R2_72_4	1442	1032.53909	1032.53909	R2_45_3	1963	4.0182492	4.0182492
R2_47_2	1201	0.007375	0.007375	R2_59_3	1083	1.057434	16.918944	R2_26_2	1417	40.484616	2.492523
R1_51_1	884	0.01475	0.04425	R1_101_1	719	11.32965	0.472075	R2_32_3	1148	4.229736	2.114868
R2_76_2	1030	0.01947	0.01947	R1_13_1	1940	113.2965	30.2124	R2_59_1	2625	4.305267	68.884272
R2_76_3	822	0.01947	0.01947	R2_6_2	491	120.8496	181.2744	R1_22_1	1169	453.186	1.888275
R2_76_1	908	0.02006	0.02006	R2_116_1	745	1.246278	1.246278	R1_14_1	664	483.3984	966.7969
R2_152_1	2243	0.0295	0.0885	R2_116_2	711	1.246278	1.246278	R1_11_1	703	483.39845	483.39845
R1_63_2	1506	0.0295	0.2065	R2_116_3	639	1.246278	1.246278	R2_150_1	755	483.39845	60.4248
R2_20_1	1258	0.02950625	0.11801875	R1_72_2	1227	1.265161	0.07906	R2_150_2	1846	483.39845	60.4248
R1_51_2	890	0.04425	0.01475	R2_72_1	1639	127.617191	127.617191	R2_19_1	1688	4.985046	2.530322
R1_21_1	867	0.0553125	0.02950625	R2_38_3	872	128.583974	128.583974	R2_60_1	1188	5.060577	39.880368
R1_93_1	1725	0.059	0.059	R1_102_1	1490	13.217925	7.5531	R2_72_3	1862	514.335951	514.335951
R1_93_2	1177	0.059	0.059	R2_14_3	931	135.351566	135.351566	R2_14_1	1069	551.074233	551.074233
R2_115_1	794	0.059	0.118	R2_24_1	3788	14.1620625	14.1620625	R1_61_2	535	5.664825	5.664825
R2_115_2	1045	0.059	0.118	R2_55_2	661	1.416225	0.118025	R1_32_1	944	56.64825	0.2360375
R2_33_1	283	0.059	0.118	R1_11_2	785	1450.19535	1450.19535	R1_92_1	1637	60.4248	15.1062
R1_24_1	4577	0.059	0.236	R2_41_1	2182	15.1062	56.64825	R1_92_2	727	60.4248	15.1062
R1_52_1	1118	0.05900625	14.1620625	R2_42_2	655	159.521472	159.521472	R2_140_1	945	60.4248	30.2124
R1_12_2	1582	0.0590125	6.6089625	R2_42_3	558	159.521472	159.521472	R1_33_1	2361	60.4248	60.4248
R2_37_2	2187	0.07788	0.01947	R1_73_1	1914	161.938464	159.521472	R1_33_2	1022	60.4248	60.4248
R2_37_3	1083	0.07788	0.01947	R2_42_1	1367	164.355456	164.355456	R1_103_1	1754	60.4248063	453.186
R2_54_1	2993	0.07788	0.15812	R2_73_2	3451	1.6522625	0.472075	R2_38_2	760	64.7753856	64.7753856
R2_37_1	1143	0.08024	0.02006	R2_53_3	1674	16.918944	135.351566	R2_57_2	1199	6.6089625	0.1180125
R2_152_2	1854	0.0885	0.0295	R2_154_2	820	1691.89458	1691.89458	R2_53_1	1916	68.884272	551.074233
R2_47_1	3894	0.110625	0.110625	R2_32_1	868	17.221068	8.610534	R2_27_2	1106	7.08103125	0.88509375
R2_105_1	375	0.118	0.059	R1_91_1	605	1.888275	113.2965	R2_7_2	1728	725.097675	15.1062
R1_82_1	1400	0.118	0.94415	R1_61_1	663	1.888275	1.888275	R1_13_2	698	7.5531	453.186
R1_82_2	982	0.118	0.94415	R1_102_2	1362	1.888275	52.8717	R1_73_2	2865	79.760736	323.876928
R1_43_1	2617	0.1180125	6.6089625	R2_68_1	2461	1.8883	0.118	R2_46_2	402	79.760736	79.760736
R2_153_3	1686	0.132174	0.066094	R2_68_2	2015	1.8883	0.118	R2_46_3	1003	79.760736	79.760736
R1_81_2	1651	0.155793	0.316307	R2_28_2	2547	19.940184	19.940184	R2_45_4	1717	8.0667108	8.0667108
R2_54_2	1523	0.15812	0.07788	R2_28_3	606	19.940184	19.940184	R2_46_1	1921	82.177728	82.177728
R1_63_1	2336	0.2065	0.0295	R2_26_1	4401	19.940184	5.060577	R2_32_2	1235	8.761596	4.380798
R1_53_1	1986	0.236	0.059	R2_45_2	1862	2.0242308	2.0242308	R1_41_1	439	90.6372	60.4248
R2_71_2	369	0.2360375	0.2360375	R2_28_1	997	20.544432	20.544432	R1_103_2	1856	906.372094	30.2124
R2_73_1	944	0.2360375	3.304525	R1_31_1	661	211.4868	211.4868	R2_65_1	908	966.7969	966.7969
R1_42_1	975	0.23605	0.23605	R2_59_2	2484	2.190399	35.046384				
R1_42_2	604	0.23605	0.23605	R2_41_2	616	226.593	3.77655				
R2_153_2	922	0.273789	0.136909	R2_154_1	912	241.699225	241.699225				
R1_83_2	945	0.311553	0.311553	R2_7_1	635	241.699225	45.3186				
R1_81_1	889	0.316307	0.155793	R2_60_2	1625	2.492523	80.969232				
R1_12_1	1310	0.4130875	0.9441375	R2_38_4	573	258.134746	258.134746				
R2_20_2	1343	0.44259375	1.77028125	R2_72_2	1792	259.101569	259.101569				
R2_27_1	2254	0.47206875	0.05900625	R1_23_1	1689	26.43585	26.43585				
R2_55_3	782	0.472075	0.354075	R1_71_2	476	26.43585	26.43585				
R2_143_1	825	0.4721	7.5531	R2_14_2	596	280.371101	280.371101				
R2_153_1	664	0.538137	0.269097	R1_91_2	954	28.324125	7.5531				
R1_72_1	988	0.623139	0.03894	R1_62_1	955	2.83245	0.236025				
R2_151_2	1000	0.623139	0.623139	R1_41_2	1001	30.2124	181.2744				
R2_151_3	492	0.623139	0.623139	R1_22_2	1041	30.2124	28.324125				
R1_83_1	1648	0.632547	0.632547	R1_31_2	1466	30.2124	30.2124				
R2_151_1	794	0.642022	0.642022	R2_117_1	1039	30.2124	30.2124				
R1_43_2	2907	0.8260875	0.9441375	R2_117_3	913	30.2124	30.2124				
R1_52_2	1504	0.88509375	0.9441375	R2_38_1	829	31.9042944	31.9042944				
R2_1_1	995	0.9441	0.9441	R2_53_2	1989	35.046384	280.371101				
R2_57_1	1392	0.9441375	0.8260875	R2_71_1	1127	3.5405625	3.5405625				
R2_24_2	2985	0.9441375	0.9441375	R2_6_1	546	362.5488	60.4248				
R1_62_2	627	0.94415	0.708075	R1_101_2	430	3.77655	1.416225				
R2_63_1	1571	0.94415	0.94415	R1_32_2	783	3.77655	3.5405625				
R2_63_3	712	0.94415	0.94415	R1_23_2	1182	3.77655	3.77655				
R2_45_1	1379	0.9970092	0.9970092	R1_71_1	825	3.77655	3.77655				
R2_19_2	6943	10.121154	1.246278	R2_67_1	523	3.7766	15.1062				

Table (S10) Sequins for differential alternative splicing events. In the table true positive sequins for alternative splicing (AS) events are shown. The two mixtures (in attomoles/μl units) with their respective concentrations are shown. Overall there are 28 true positive sequins for AS events. The saffron colored sequins are true positive, however these were consistently found to be of low coverage regardless of the aligner used for alignment (see Appendix Table). Not to penalize AS event detection tools, the true positive sequins were reset to 22 counts. Sequins with one isoform or no change in ratios across the two mixtures were our true negative. We don't expect these sequins to be reported by any AS tools. Appendix Figure S3 and Figure S4 show the read coverage from two aligners (STAR and HISAT2).

GeneID	IsoformID	Length	MixA	MixB
R1_101	R1_101_1	719	11.32965	0.472075
	R1_101_2	430	3.77655	1.416225
R1_102	R1_102_1	1490	13.217925	7.5531
	R1_102_2	1362	1.888275	52.8717
R1_103	R1_103_1	1754	60.4248063	453.186
	R1_103_2	1856	906.372094	30.2124
R1_12	R1_12_1	1310	0.4130875	0.9441375
	R1_12_2	1582	0.0590125	6.6089625
R1_13	R1_13_1	1940	113.2965	30.2124
	R1_13_2	698	7.5531	453.186
R1_21	R1_21_1	867	0.0553125	0.02950625
	R1_21_2	794	0.0036875	0.44259375
R1_22	R1_22_1	1169	453.186	1.888275
	R1_22_2	1041	30.2124	28.324125
R1_32	R1_32_1	944	56.64825	0.2360375
	R1_32_2	783	3.77655	3.5405625
R1_41	R1_41_1	439	90.6372	60.4248
	R1_41_2	1001	30.2124	181.2744
R1_43	R1_43_1	2617	0.1180125	6.6089625
	R1_43_2	2907	0.8260875	0.9441375
R1_51	R1_51_1	884	0.01475	0.04425
	R1_51_2	890	0.04425	0.01475
R1_52	R1_52_1	1118	0.05900625	14.1620625
	R1_52_2	1504	0.88509375	0.9441375
R1_62	R1_62_1	955	2.83245	0.236025
	R1_62_2	627	0.94415	0.708075
R1_63	R1_63_1	2336	0.2065	0.0295
	R1_63_2	1506	0.0295	0.2065
R1_73	R1_73_1	1914	161.938464	159.521472
	R1_73_2	2865	79.760736	323.876928
R1_81	R1_81_1	889	0.316307	0.155793
	R1_81_2	1651	0.155793	0.316307
R1_91	R1_91_1	605	1.888275	113.2965
	R1_91_2	954	28.324125	7.5531
R2_152	R2_152_1	2243	0.0295	0.0885
	R2_152_2	1854	0.0885	0.0295
R2_19	R2_19_1	1688	4.985046	2.530322
	R2_19_2	6943	10.121154	1.246278
R2_26	R2_26_1	4401	19.940184	5.060577
	R2_26_2	1417	40.484616	2.492523
R2_41	R2_41_1	2182	15.1062	56.64825
	R2_41_2	616	226.593	3.77655
R2_54	R2_54_1	2993	0.07788	0.15812
	R2_54_2	1523	0.15812	0.07788
R2_55	R2_55_2	661	1.416225	0.118025
	R2_55_3	782	0.472075	0.354075
R2_57	R2_57_1	1392	0.9441375	0.8260875
	R2_57_2	1199	6.6089625	0.1180125
R2_6	R2_6_1	546	362.5488	60.4248
	R2_6_2	491	120.8496	181.2744
R2_60	R2_60_1	1188	5.060577	39.880368
	R2_60_2	1625	2.492523	80.969232
R2_7	R2_7_1	635	241.699225	45.3186
	R2_7_2	1728	725.097675	15.1062
R2_73	R2_73_1	944	0.2360375	3.304525
	R2_73_2	3451	1.6522625	0.472075

Table (S11) Sequins missed by the DTE tools. The expected absolute log-fold-change values of each sequins is shown in the table.

Sequins	Total_Isoform	Kallisto	EBSeq	LFC	Tissue
R1_51	2	Not Reported	Not Reported	1.5	Brain, Kidney, Muscle, Retina, RPE
R1_81	2	Not Reported	NA	1.02	Brain
R1_61	2	Not Reported	NA	0.4	Muscle
R1_21	2	Not Reported	Not Reported	6.90	Retina
R2_115	2	Not Reported	Not Reported	1	RPE
R2_54	2	Not Reported	Not Reported	1.02	RPE

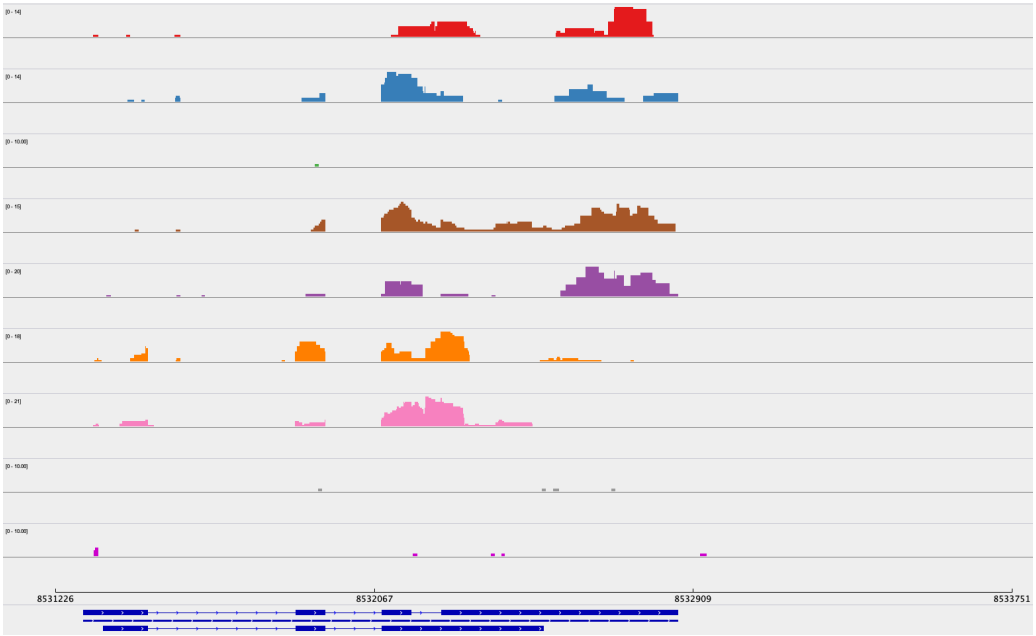

Figure (S3) Sashimi plot for true positive sequin using STAR on mouse brain samples. This sequin, R1_62 is not among the lowest concentration of sequin (8th highest concentration) gene. This sequin is not well covered by the aligner.

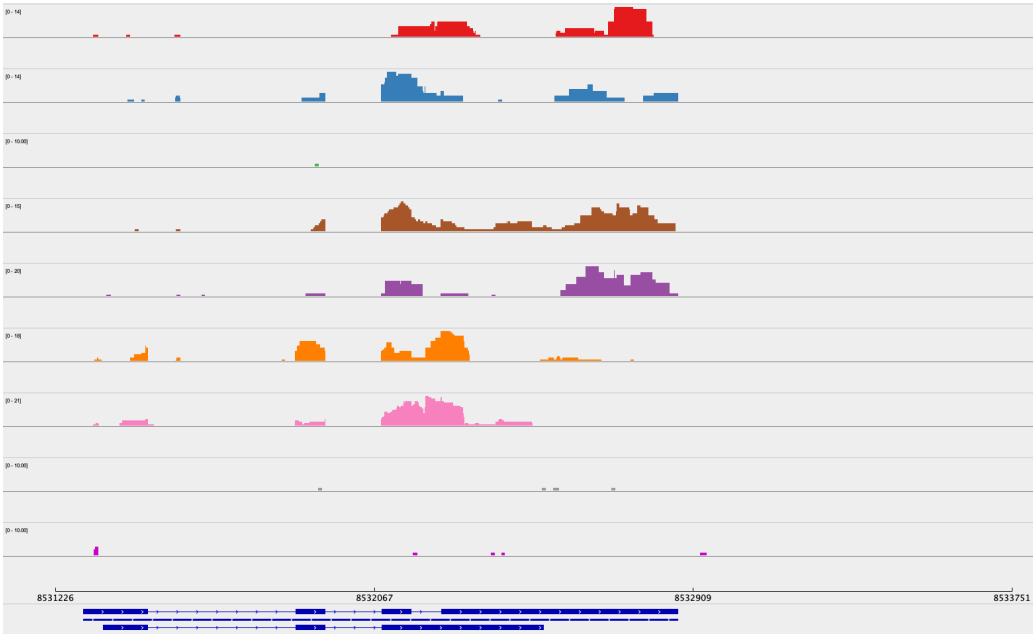

Figure (S4) Sashimi plot for true positive sequin using HISAT2 on mouse brain samples. This sequin, R1_62 is not among the lowest concentration of sequin (8th highest concentration) gene. This sequin is not well covered by the aligner.

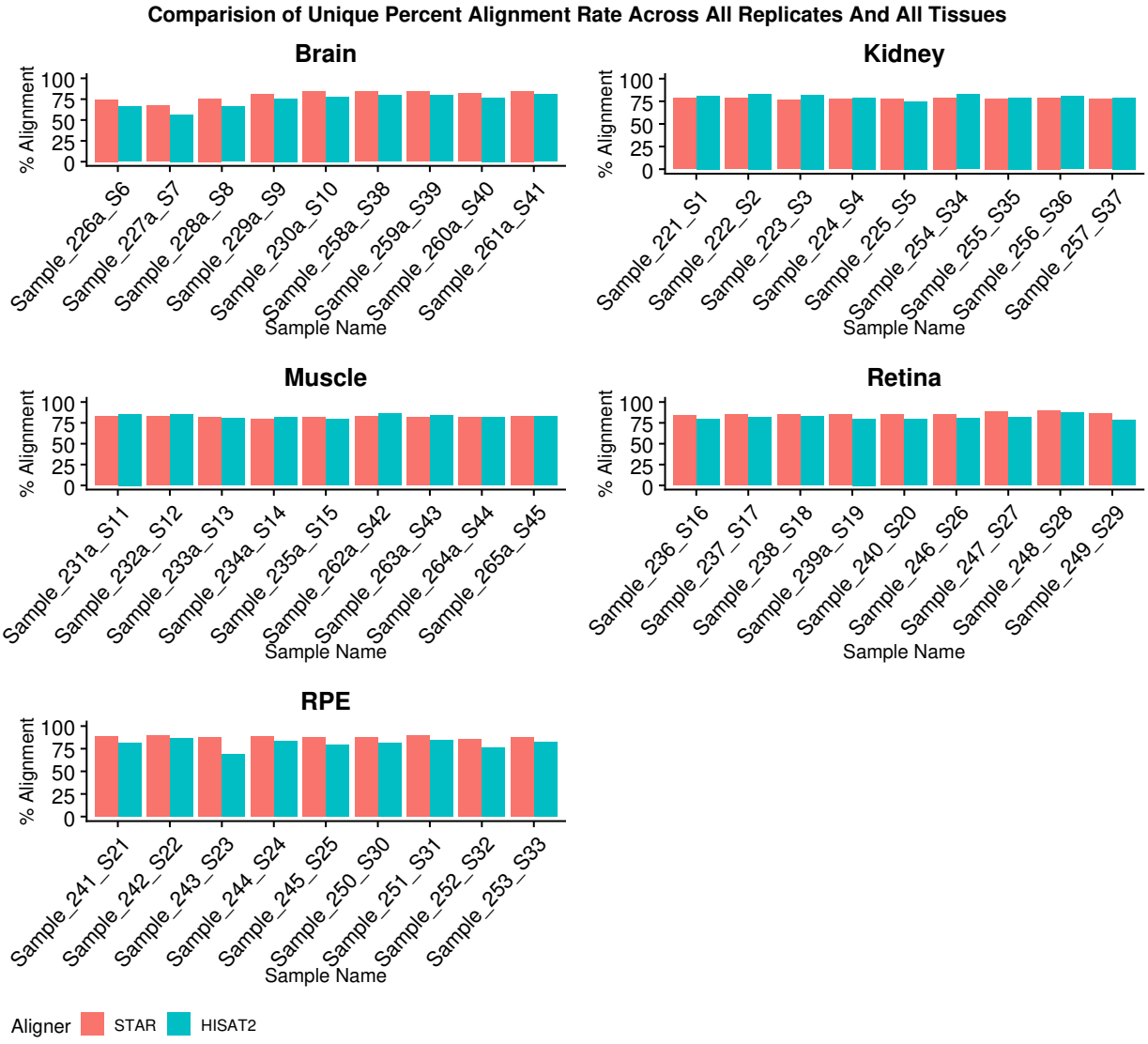

Figure (S5) Comparative alignment rate from the two aligners for all the reads. The figure shows percentage unique alignment as reported by STAR and HISAT2 for all the five mouse tissues. Over all the alignment rates were indistinguishable. Assigned unique sample identifier assigned to each sample is shown in the x-axis and percentage alignment rate on y-axis. From left to right, first 5 are mutants followed by wild type samples.

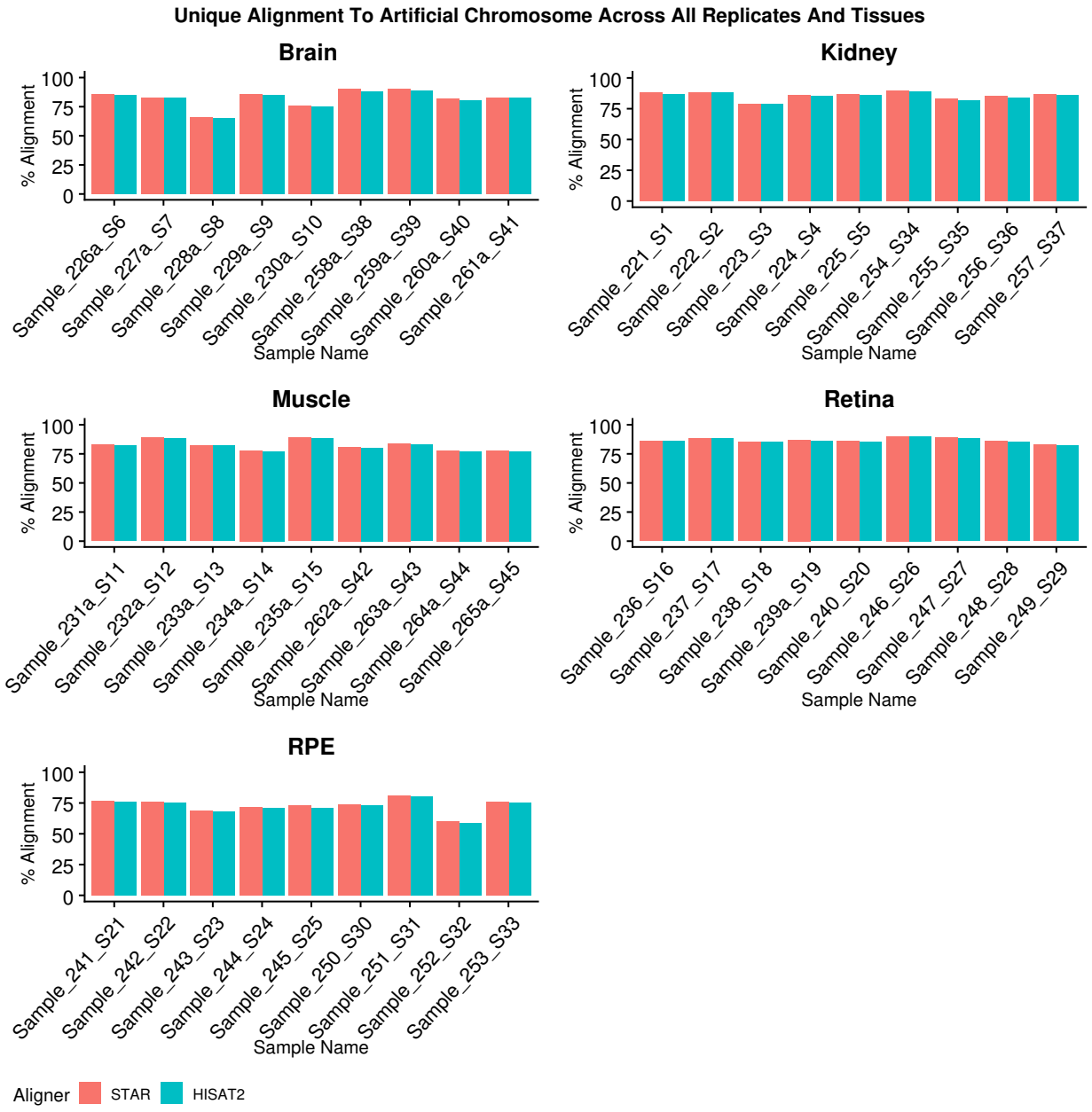

Figure (S6) Comparative *IS* specific alignment rate from the two aligners. The figure shows percentage unique alignment specific to the spiked-in *in-silico* artificial chromosome (IS) as reported by STAR and HISAT2 for all the five mouse tissues. The alignment rates were indistinguishable. Assigned unique sample identifier assigned to each sample is shown in the x-axis and percentage alignment rate on y-axis.

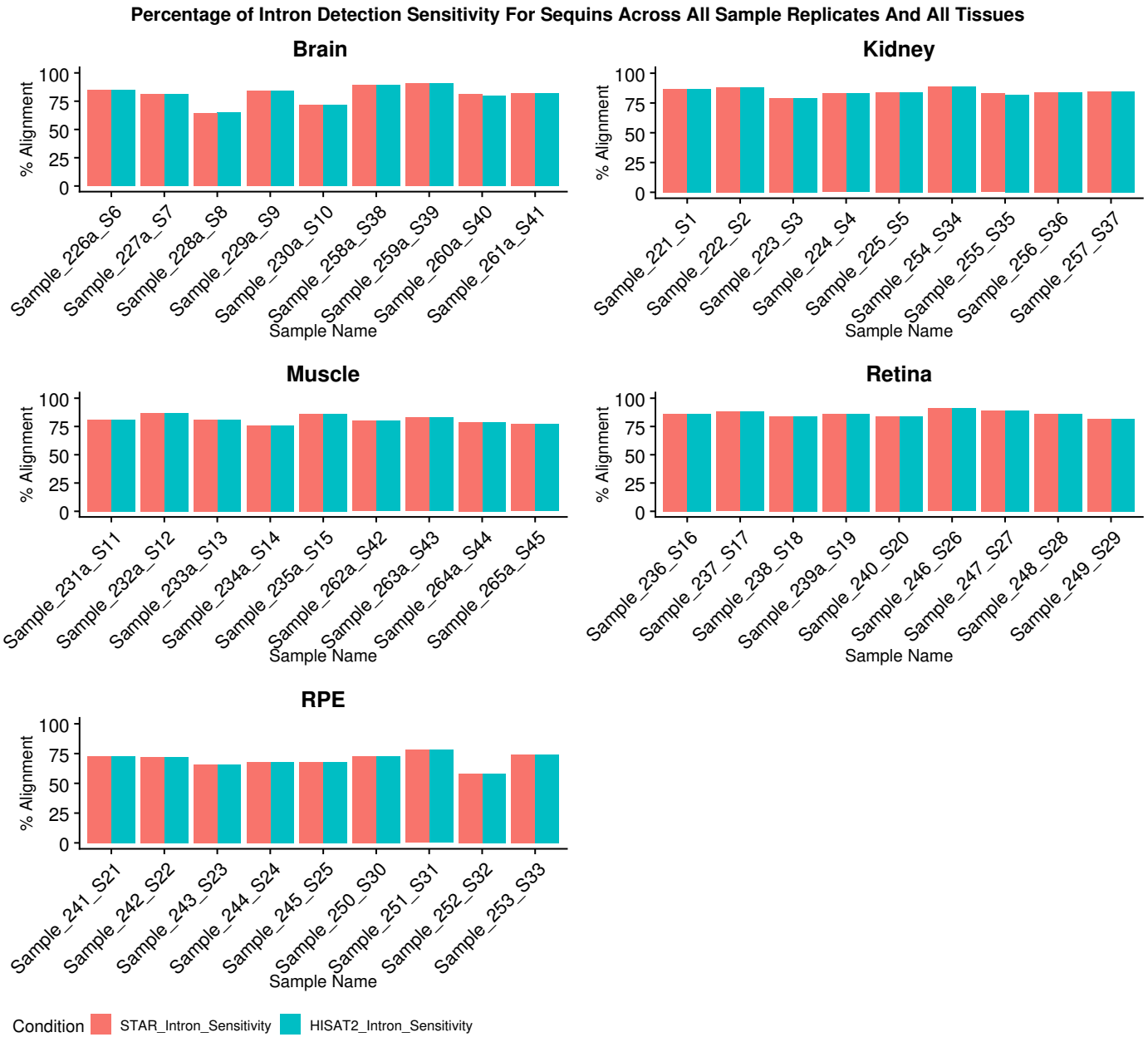

Figure (S7) Comparative intron sensitivity for the two aligners. The figure shows intron sensitivity rate as reported by STAR and HISAT2 for all the five mouse tissues using Anaquin. Sensitivity indicates the fraction of annotated regions covered by alignments of the reads. The alignment rates were indistinguishable. From left to right, first 5 are mutants followed by wild type samples.

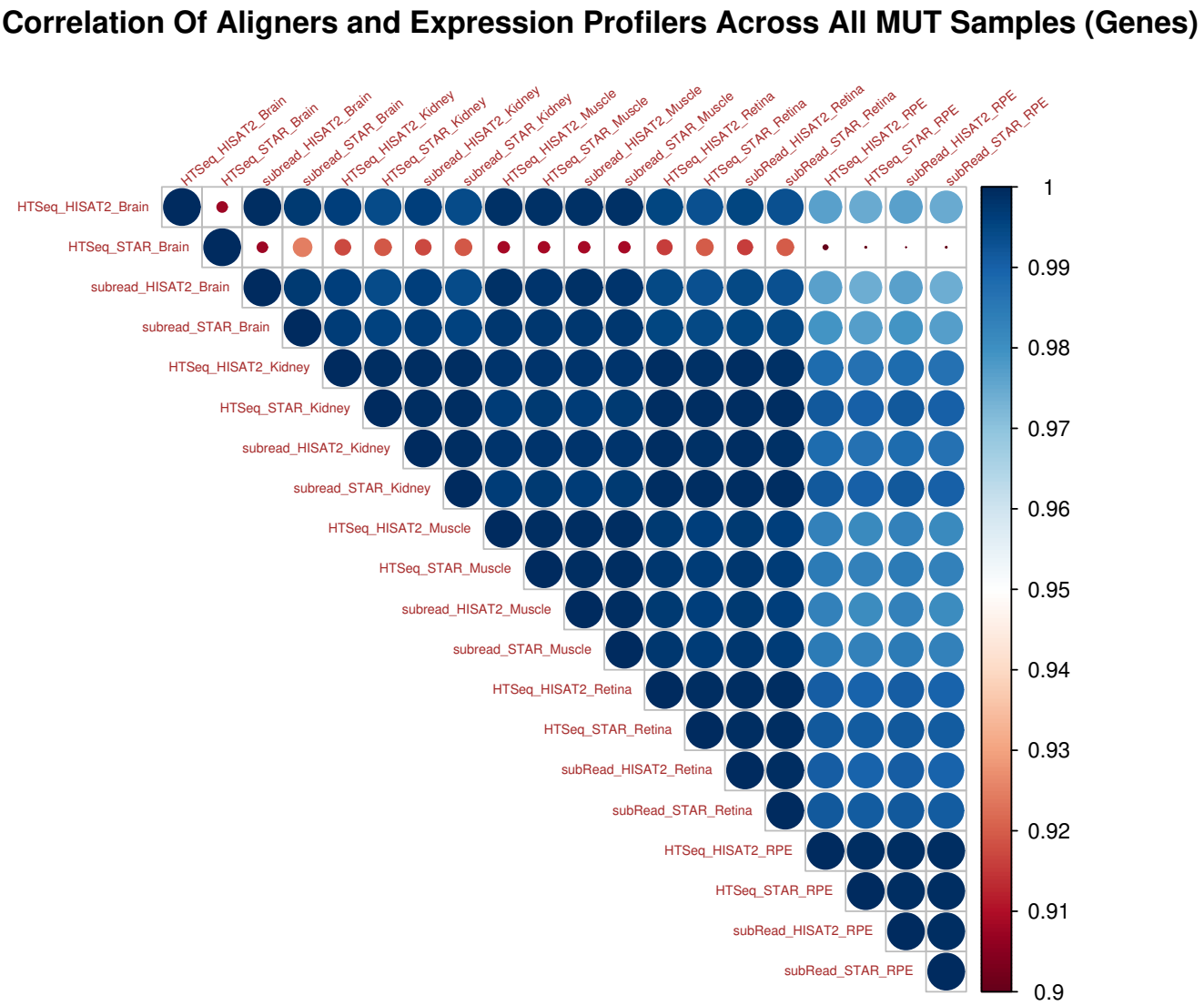

Figure (S8) Correlation plot for comparative analysis across all the mutant type tissues. An upper triangular heatmap shows high correlation across different combination of the aligners and read counting tools across the five mouse tissues and their replicates. The average TPM values across the replicates were used to calculate the Pearson correlation.The combinations of tools used are shown in the format of: Gene Expression Profile_Aligner_Tissue.

The following analysis tool combinations were identified (the combination of tools are listed as DGE_aligner_gene expression profile tool, along with missing number of sequin genes in brackets) edgeR_STAR_fC (1), edgeR_STAR_HTC (3), DESeq2_STAR_fC (1) and DESeq2_STAR_HTC (3). Here, fC refers to featureCount and HTC refers to HTSeq-Counts. Similarly, for the kidney sample, the same combinations of analysis tools; edgeR_STAR_fC (1), edgeR_STAR_HTC(1), DESeq2_STAR_fC (1) and DESeq2_STAR_HTC (1) showed drop in performance. The same unary sequin gene, identified in the brain samples, was also not reported in the kidney samples.

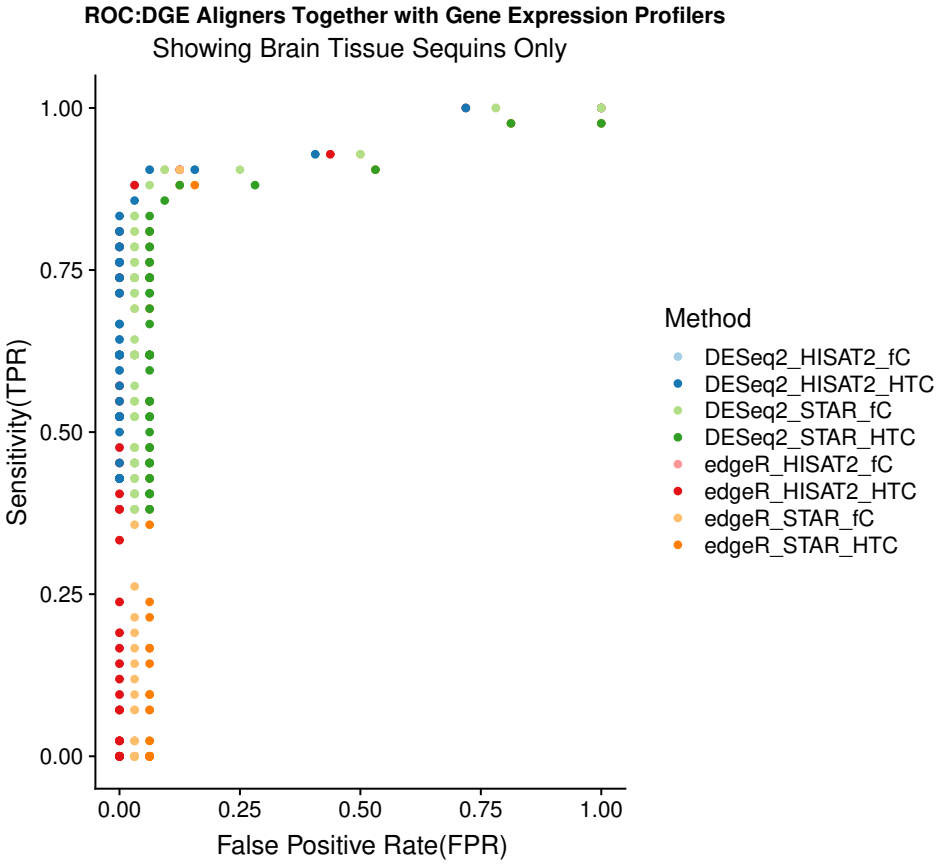

Figure (S9) ROC (receiver operating characteristic) curves for Sequin genes for diagnostic performance in mouse brain tissue. The following tools, presented in the form of is DGE_aligner_gene expression profile tool showed poor performance (in brackets total count of missed sequin gene is shown): edgeR_STAR_fC (1), edgeR_STAR_HTC (3), DESeq2_STAR_fC (1) and DESeq2_STAR_HTC (3) compared to rest of the combinations.

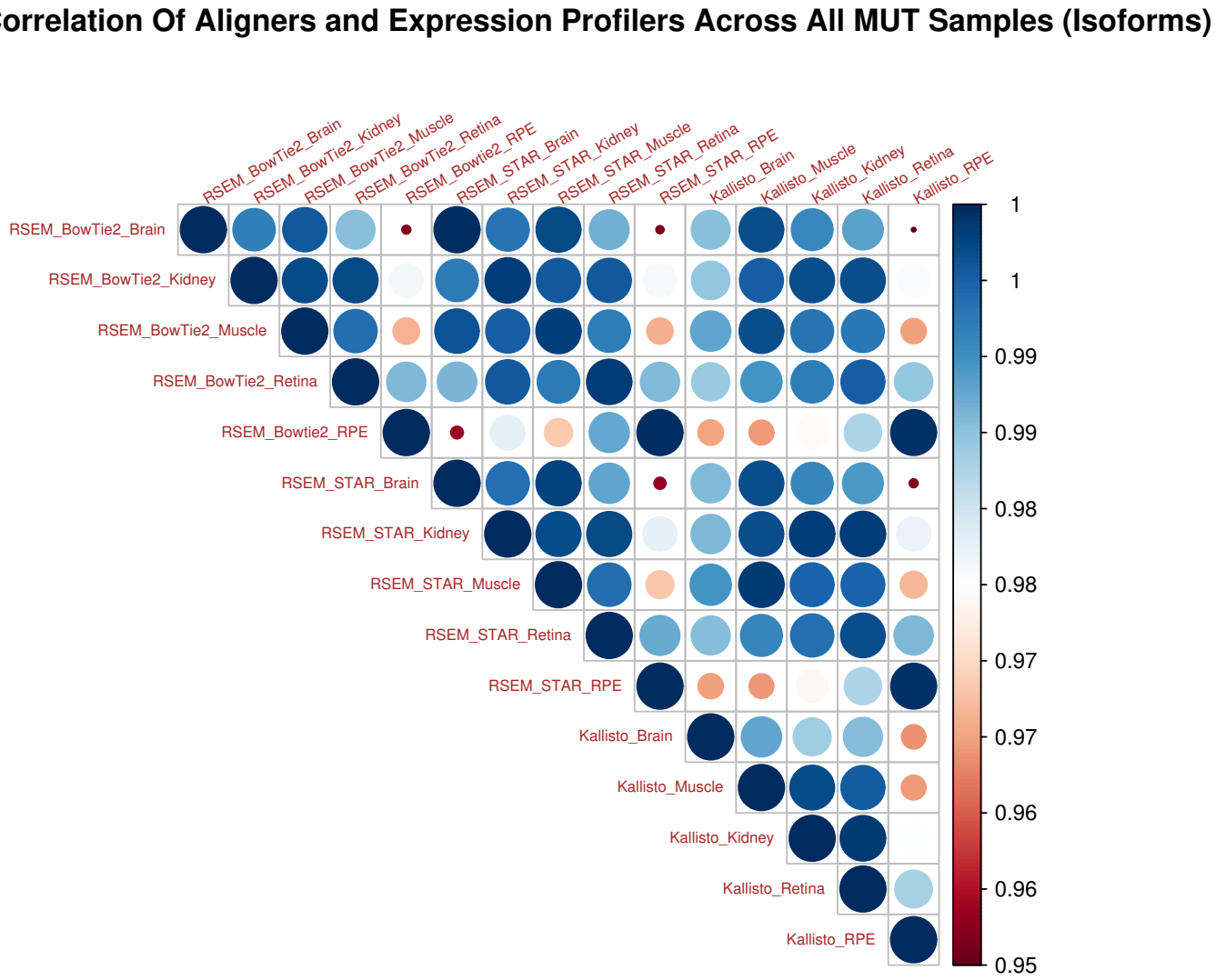

Figure (S10) Correlation plot for comparative analysis for all the mutant samples using RSEM and two aligners along with Kallisto across all the mouse tissues. An upper triangular heatmap is generated showing Pearson correlation of determination values using average TPM expression values across the five mouse tissues. The combinations of tools used are shown in the format of: ExpressionTool_Aligner_Tissue, for example, RSEM_STAR_Brain. High correlation of determination values were observed across different tissues types and combinations of different tools.

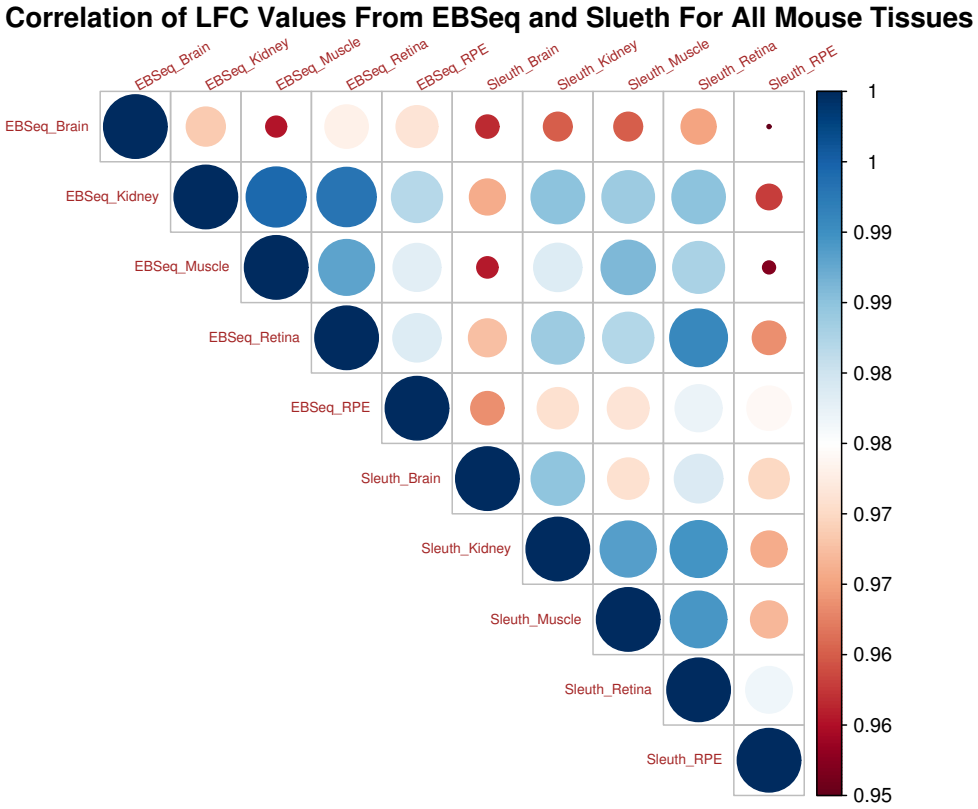

Figure (S11) Correlation for differential isoform expression across all five tissues using EBSeq and Kallisto. High correlation was observed for sequins reported by both the tools. We used a "complete case analysis" approach and removed sequins not reported by either of the programs. Refer to Figure S12 for impacts of directionality and proportions and Figure 10 shows sensitivity and specificity including impacts due to missed sequin isoforms.

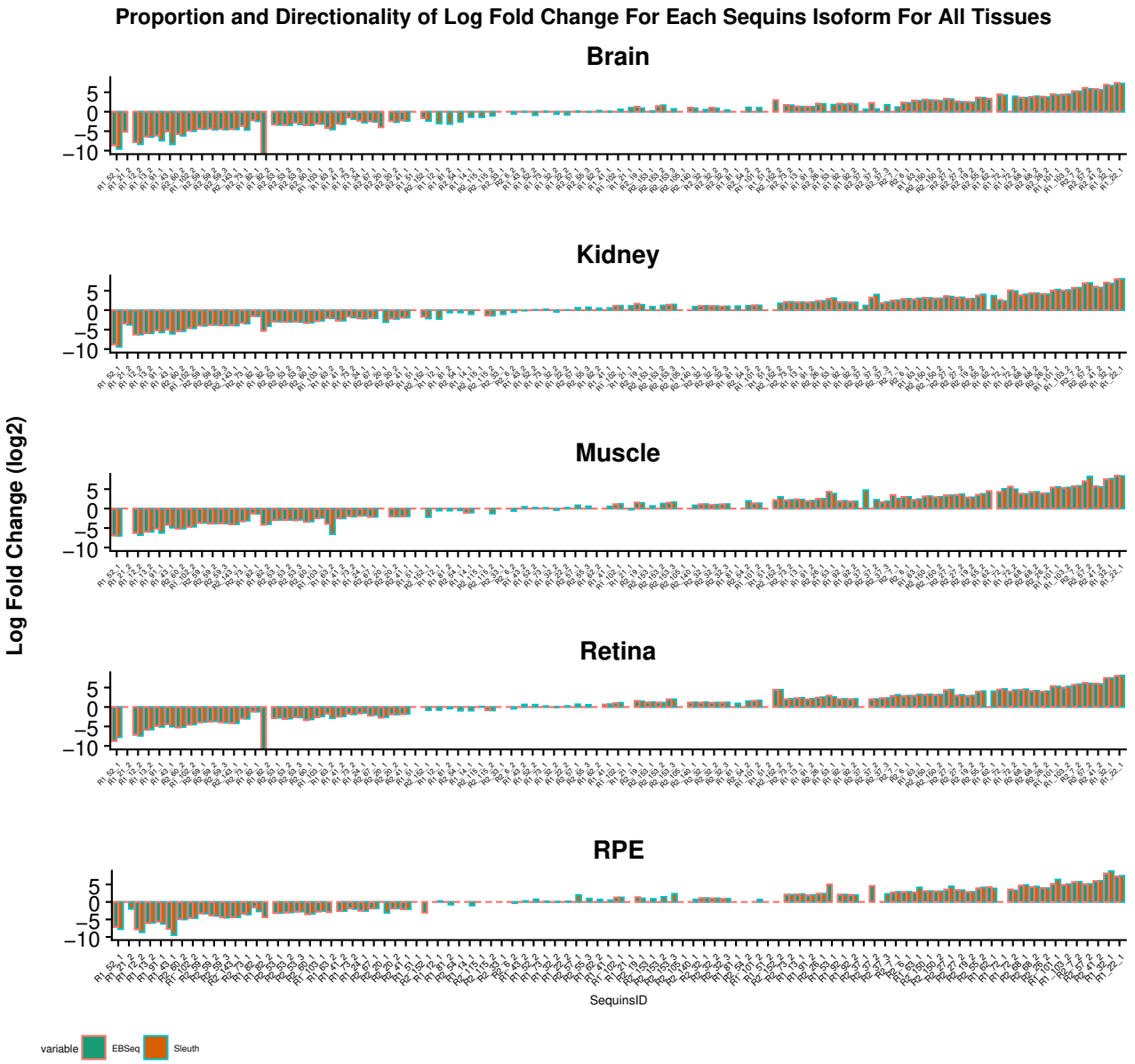

Figure (S12) Comparative proportion of log-fold-changes for the sequin genes across all the mouse tissues using different tools. RSEM with default aligner(Bowtie2) was used in conjunction with EBSeq for differential isoform expression. The combined pipeline of Kallisto and Sleuth was used. In the x-axis all the sequin genes are shown and on the y-axis LFC values (log2) are shown. The sequin identifiers are sorted based on expected LFC values and are static all across the tissues. For all mouse tissues, Sleuth and EBSeq missed to report both the isoforms for one sequins. Overall in the brain 4 sequin isoforms, 2 in kidney, 4 in muscle and retina and 6 in RPE were not reported by Kallisto. Similarly, 2 isoforms in the retina and 4 in RPE were not reported by EBSeq. See Table S11 for more details.

Table (S12) Sequins sensitivity from two aligners. The table shows counts of AS events from STAR and HISAT2. MAJIQ was used for AS detection. In the mouse retina and brain the percent sensitivity from HISAT2 was slightly higher than STAR. Absence of unary sequins from STAR made the difference in favor of HISAT. In all the other cases it was identical. In caption H refers to HISAT2 and S refers to STAR aligner.

	RPE_H	RPE_S	Retina_H	Retina_S	Brain_H	Brain_S	Muscle_H	Muscle_S	Kidney_H	Kidney_S
TP	15	15	20	19	14	13	17	17	20	20
FN	7	7	2	3	8	9	5	5	2	2
Sensitivity%	68.18	68.18	90.90	86.36	63.63	59.09	77.27	77.27	90.90	90.90

Table (S13) Sequins sensitivity and specificity from two aligners with JunctionSeq. The table shows counts of AS events from STAR and HISAT2. JunctionSeq was used for AS detection. With exception of reporting of higher false positives for retina samples (5), and muscle (2) near identical results were observed between the two aligners. In caption H refers to HISAT2 and S refers to STAR aligner.

	RPE_H	RPE_S	Retina_H	Retina_S	Brain_H	Brain_S	Muscle_H	Muscle_S	Kidney_H	Kidney_S
TP	20	19	22	22	22	22	22	22	22	22
FN	2	3	0	0	0	0	0	0	0	0
Sensitivity%	90.90	86.3	100	100	100	100	100	100	100	100
TN	46	46	42	46	46	46	45	47	46	47
FP	1	1	5	1	1	1	2	0	1	0
Specificity%	97.87	97.87	89.36	97.87	97.87	97.87	95.74	100	97.87	100

Table (S14) Novel splice junctions on sequins by two aligners with JunctionSeq. Novel splice junctions on sequins were observed across all the tissues by both the aligners. We noticed reports of novel splice junctions on sequins, more from the STAR aligner. Three (3) was the max number of novel splice junction per gene. SJ refers to splice junctions. Use of STAR aligner with the tissue is marked and unmarked is with HISAT2

Tissue/Junctions	RPE STAR	RPE	Retina STAR	Retina	Brain STAR	Brain	Kidney STAR	Kidney	Muscle STAR	Muscle
Total_Novel_SJ	1	0	6	3	4	1	6	3	5	1

Table (S15) Metrics associated with downsampling mouse RPE sample set. The table shows a number of metrics: original genomic read counts, unique read counts, sequins (IS) read counts, expected IS reads and actual IS reads pre and post downsampling. There were samples that do not meet the minimum read count requirement, such samples were used entirely and thus "NA" is marked where appropriate.

Sample/Metrics	Sample_241	Sample_242	Sample_243	Sample_244	Sample_245	Sample_250	Sample_251	Sample_252	Sample_253
Total Genomic Reads	171,277,676	136,971,381	43,860,070	105,820,965	99,669,330	83,863,562	180,409,737	12,341,074	172,423,806
Total Unique	156,862,596	127,822,132	39,508,253	96,366,828	90,026,821	77,264,930	167,769,135	10,946,126	156,697,562
Goal	150,000,000	NA	NA	NA	NA	NA	150,000,000	NA	150,000,000
Total IS	6,439,631	5,248,821	1,294,470	3,461,062	3,465,795	4,257,131	7,324,428	391,270	6,066,618
ExpectedInDown(IS)	5639641	NA	NA	NA	NA	NA	6089827	NA	5277651
ActualPostDown(IS)	5,640,181						6,086,911		5,277,773
Goal	100,000,000	100,000,000	NA	NA	NA	NA	100,000,000	NA	100,000,000
ExpectedInDown	3,759,761	3,832,057					4,059,885		3,518,434
ActualPostDownSample	3,761,086	3,833,282					4,276,759		3,542,108
Goal	50,000,000	50,000,000	NA	50,000,000	50,000,000	50,000,000	50,000,000	NA	50,000,000
ExpectedInDown	1,879,880	1,916,028		1,635,339	1,738,647	2,538,129	2,029,943		1,759,217
ActualPostDownSample	1,878,426	1,917,826		1,634,916	1,739,003	2,536,888	2,026,548		1,761,394

Table (S17) Metrics associated with downsampling mouse brain sample set. The table shows a number of metrics: original genomic read counts, unique read counts, sequins (IS) read counts, expected IS reads and actual IS reads pre and post downsampling. There were samples that do not meet the minimum read count requirement, such samples were used entirely and thus "NA" is marked where appropriate.

Sample/Metrics	Sample_226a	Sample_227a	Sample_228a	Sample_229a	Sample_230a	Sample_258a	Sample_259a	Sample_260a	Sample_261a
Total Genomic Reads	224,175,418	298,289,266	254,811,577	167,382,931	143,008,334	228,263,098	193,227,601	212,318,905	188,721,455
Total Unique	172,297,176	206,280,820	195,104,137	142,045,086	124,327,978	205,547,310	175,360,125	181,166,892	165,768,006
Goal	150,000,000	150,000,000	150,000,000	150,000,000	NA	150,000,000	150,000,000	150,000,000	150,000,000
Total IS	7,395,267	7,727,831	3,239,520	6,757,306	3,998,469	15,226,593	15,045,437	8,656,728	7,005,287
ExpectedInDown(IS)	4,948,313	3,886,076	1,907,009	6,055,551	NA	10,005,949	11,679,571	6,115,844	5,567,958
ActualPostDown(IS)	4,947,822	3,883,978	1,907,141	6,056,207		10,008,758	11,673,649	6,115,210	5,568,327
Goal	100,000,000	100,000,000	100,000,000	100,000,000	100,000,000	100,000,000	100,000,000	100,000,000	100,000,000
ExpectedInDown(IS)	3,298,875	2,590,717	1,271,339	4,037,034	2,795,969	6,670,633	7,786,381	4,077,229	3,711,972
ActualPostDown(IS)	3,299,817	2,591,329	1,271,553	4,037,572	2,795,638	6,669,839	7,783,162	4,076,058	3,709,669
Goal	50,000,000	50,000,000	50,000,000	50,000,000	50,000,000	50,000,000	50,000,000	50,000,000	50,000,000
ExpectedInDown(IS)	1,649,438	1,295,359	635,670	2,018,517	1,397,985	3,335,316	3,893,190	2,038,615	1,855,986
ActualPostDown(IS)	1,648,941	1,297,001	637,197	2,018,611	1,396,598	3,335,296	3,897,183	2,039,186	1,855,929

Table (S16) Metrics associated with downsampling mouse retina sample set. The table shows a number of metrics: original genomic read counts, unique read counts, sequins (IS) read counts, expected IS reads and actual IS reads pre and post downsampling. There were samples that do not meet the minimum read count requirement, such samples were used entirely and thus "NA" is marked where appropriate

Sample/Metrics	Sample_236	Sample_237	Sample_238	Sample_239a	Sample_240	Sample_246	Sample_247	Sample_248	Sample_249
Total Genomic Reads	179,710,867	202,798,068	139,679,922	172,407,601	137,407,045	239,497,635	203,542,171	188,923,358	150,278,217
Total UniqueReads	156,960,473	178,562,546	124,283,827	152,415,475	123,087,638	214,946,863	188,611,822	177,222,027	134,343,354
Goal	150,000,000	150,000,000	NA	150,000,000	NA	150,000,000	150,000,000	150,000,000	NA
Total IS	6,503,186	7,544,866	6,868,886	6,450,277	7,167,630	13,673,884	10,238,750	9,498,976	5,496,948
ExpectedInDown(IS)	5,428,041	5,580,575	NA	5,611,943	NA	8,564,104	7,545,427	7,541,928	NA
ActualPostDown(IS)	5,427,538	5,581,853		5,611,494		8,564,204	7,546,849	7,542,031	
Goal	100,000,000	100,000,000	100,000,000	100,000,000	100,000,000	100,000,000	100,000,000	100,000,000	100,000,000
ExpectedInDown(IS)	3618693	3720383	4917590	3741295	5216348	5709402	5030284	5027952	3657847
ActualPostDown(IS)	3,618,070	3,719,887	4,919,517	3,738,769	5,219,733	5,711,413	5,029,642	5,027,127	3,656,115
Goal	50,000,000	50,000,000	50,000,000	50,000,000	50,000,000	50,000,000	50,000,000	50,000,000	50,000,000
ExpectedInDown(IS)	1809346	1860191	2458795	1870647	2608174	2854701	2515142	2513976	1828923
ActualPostDown(IS)	1,808,600	1,860,175	2,459,651	1,869,461	2,605,755	2,854,939	2,515,147	2,516,084	1,826,335

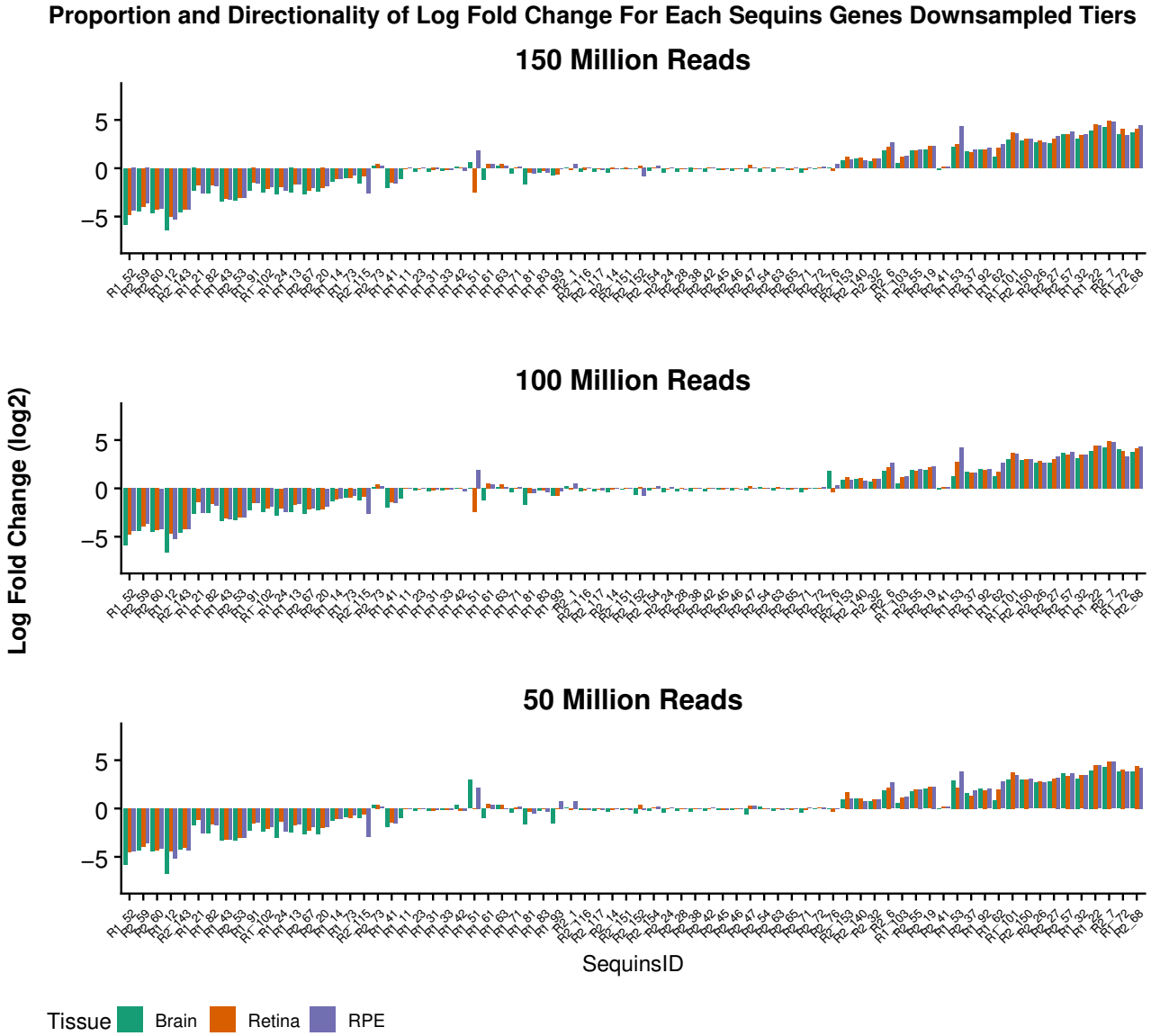

Figure (S13) Proportionality and directionality of the downsampled data. The x-axis shows all the sequin genes and y-axis represents the observed LFC values. The observed LFC and directionality for sequin genes across all the three titers is shown. Comparable results were observed regardless of the random read set. As observed with complete read set, sequin genes between -1–+1 showed more variations than the other LFC values. A maximum of 1 sequins were lost. For example, in the 150 million read set, R2_76 in brain and R2_54 in RPE were not reported. In the 100 million read set, R2_54 was not reported in the RPE. In the 50 million read set, R1_51 in retina, R2_54 in RPE and R2_76 in brain and RPE were not reported.